Blue-Green Luminescence from $CsPbX_3$ perovskite nanocrystals (X = Br, Cl, Br/Cl)

A thesis submitted to

Indian Institute of Science Education and Research (IISER), Pune

in partial fulfilment of the requirements for the BS-MS Dual Degree Programme

by

Sreejith P Nandan

Reg. No: 20111065

Under the supervision of

Dr. Angshuman Nag

Assistant professor,

Department of Chemistry, IISER Pune

April 2016

Certificate

This is to certify that this dissertation entitled "Blue-Green Luminescence from $CsPbX_3$ perovskite nanocrystals (X = Br, Cl, Br/Cl)" towards the partial fulfilment of the BS-MS dual degree programme at the Indian Institute of Science Education and Research, Pune represents the research carried out by Sreejith P Nandan at IISER Pune under the supervision of Dr. Angshuman Nag, Assistant Professor, IISER Pune during the academic year 2015-2016.

Date: 28/04/2016

Place: Pune

Angshuman Nag

Dr. Angshuman Nag,
Assistant Professor,
IISER Pune.

Declaration

I hereby declare that the matter embodied in the report entitled "Blue-Green Luminescence from $CsPbX_3$ perovskite nanocrystals (X = Br, Cl, Br/Cl)" are the results of the investigations carried out by me at the Department of Chemistry, IISER Pune, under the supervision of Dr. Angshuman Nag and the same has not been submitted elsewhere for any other degree.

Date: 28-04-2016

Place: Pune.

Sreejith P Nandan
20111065
B.S – M.S Student
IISER Pune

Abstract

CdSe based traditional colloidal quantum dots (cQDs) are well known for their photoluminescence (PL) properties. Last year, colloidal $CsPbBr_3$ nanocrystals (NCs), that has nearly ideal quantum yield (QY) of ~90% with narrow (FWHM = 85 meV) spectral width was reported. Later, it was demonstrated that $CsPbBr_3$ NCs have less influence of self-absorption and Förster resonance energy transfer (FRET). Furthermore, they exhibit no change in the PL peak position in the temperature range of 25 ^oC to 100 ^oC. But these properties were mainly established for emission with peak at 511 nm. The motive of my work is to extend the emission range to lower wavelengths without compromising on these exciting properties. Size-dependent tuning of the emission wavelengths is inhibited for $CsPbBr_3$ NCs as it doesn't lie in quantum confinement (QC) regime. So, tuning can be achieved by compositional modulation of $CsPbX_3$ (X = Cl, Br, I or Cl/Br, Br/I) NCs. Surprisingly, colloidal $CsPbX_3$ (X = Br, Cl, Br/Cl) NCs show either no change or a slight blue shift (upto 2-3 nm) in the PL peak position with variation of temperature from 20 ^oC to 80 ^oC. Interestingly, a high PL QY (55-80%) along with narrow FWHM (75-95 meV) is obtained in blue-green emission with PL peak ranging between 465 to 515 nm. It is to be noted that achieving high PL QY for blue emitting QDs have been an outstanding problem for a long time. Another important aspect is that the PL decay dynamics of $CsPbX_3$ NC films show similar decay at all emission energies, which suggest less influence of FRET in chromaticity.

Table of Contents

List of Figures

List of Tables

Acknowledgement

First and foremost, I thank Dr. Angshuman Nag for his wonderful mentoring, for all the fruitful discussions and for his encouragement and motivation throughout the project tenure. He entrusted me with an independent, fast- growing, and exciting project even though I am a beginner in research, and I am really grateful to him for having so much faith in me. I also thank Dr. Pankaj Mandal for co-mentoring me during the project and for his constructive suggestions during the whole year. I would like to thank Abhishek for establishing a great system to work on and also for helping out with reactions when I started. I thank Vikash for he was a constant support for my project. I want to thank Jagadeesh, Shiva, Wasim and Kiran for all the discussions and brainstorming, which helped me grow a lot. I thank Bharat for his helping hand in EDAX measurements. I thank Anur for all the talks we used to have, both inside and outside the lab and more than that for being a great friend. I also thank Jaya, Ganesh, Pranavi, Rayan and Ashutosh for creating a light and happy atmosphere to work in.

I am really grateful to my family for being very understanding and for keeping me happy at every step in the journey, without whom completion of this project would have been impossible. I can't thank them enough for all the encouragement and for being there with me. Thanks to all my friends and beloved ones.

Chapter-1: Introduction

In recent times, metal halide perovskites are of huge interest because of their high efficiency in solar cells as an active layer[1]. With the help of solution processed hybrid perovskites like $CH_3NH_3PbI_3$, solar cell efficiencies have increased to ~22% by now and has become a promising candidate for real life applications[2][3]. This led to a further study on hybrid metal halide perovskites for various opto-electronic properties and their competency in Light emitting diodes (LEDs)[4], Field effect transistors (FETs)[5] UV-Vis photodetectors[6] etc. has already been reported. Later, research was also undertaken to study photoluminescence (PL) of hybrid organic-inorganic perovskite nanocrystals (NCs) such as $CH_3NH_3PbX_3$ (X = Br, Cl, I or mixed systems like Br/Cl, Br/I) NCs[7][8].

The first synthesis of fully inorganic metal halide perovskites such as $CsPbX_3$ dates back to 1958 when Möller reported the crystal structure and photoconductivity of Cesium lead trihalides[7]. Since then, many interesting properties of bulk inorganic metal halides have been reported.

Properties of bulk $CsPbBr_3$

$CsPbBr_3$ is a direct band gap material. Bulk $CsPbBr_3$ shows PL emission at low temperatures like 6 K with small Stoke's shift between excitation and emission spectra. As the temperature increases, PL intensity starts decreasing and it almost becomes negligible as it reaches 90 K[10]. So, room temperature PL is not observed for bulk $CsPbBr_3$. The emission spectra at 533 nm is attributed to free Wannier exciton and it shows an extremely fast decay; having lifetime of 10-20 ps. The reason for the fast decay could be an effective non-radiative energy transfer to trap states, that in turn decreases the exciton duration in the excited state[10].

Colloidal $CsPbX_3$ NCs

Having a wide bulk band gap and direct band-to-band transition (determined from the band structure calculations)[11]; $CsPbBr_3$ or $CsPbX_3$ (where X = Br, Cl) in general, can be a good system to look for Quantum confinement (QC) effect, i.e. when the size of nanocrystals is comparable to that of Bohr-exciton radius[12]. Recently with such an

immense success of hybrid perovskites, synthesis of all inorganic $CsPbX_3$ (X = Br,Cl, I) NCs became a hot question to address.

Last year, Protesescu et al. for the first time reported synthesis of monodisperse, colloidal NCs of fully inorganic Cesium lead halide perovskites $CsPbX_3$ (X= Cl, Br, I or mixed systems Cl/Br and Br/I)[13]. They also showed that by compositional modulation, the band gap energies and emission spectra are tunable over the entire visible region (410-700 nm) as shown in the Figure 1.1.

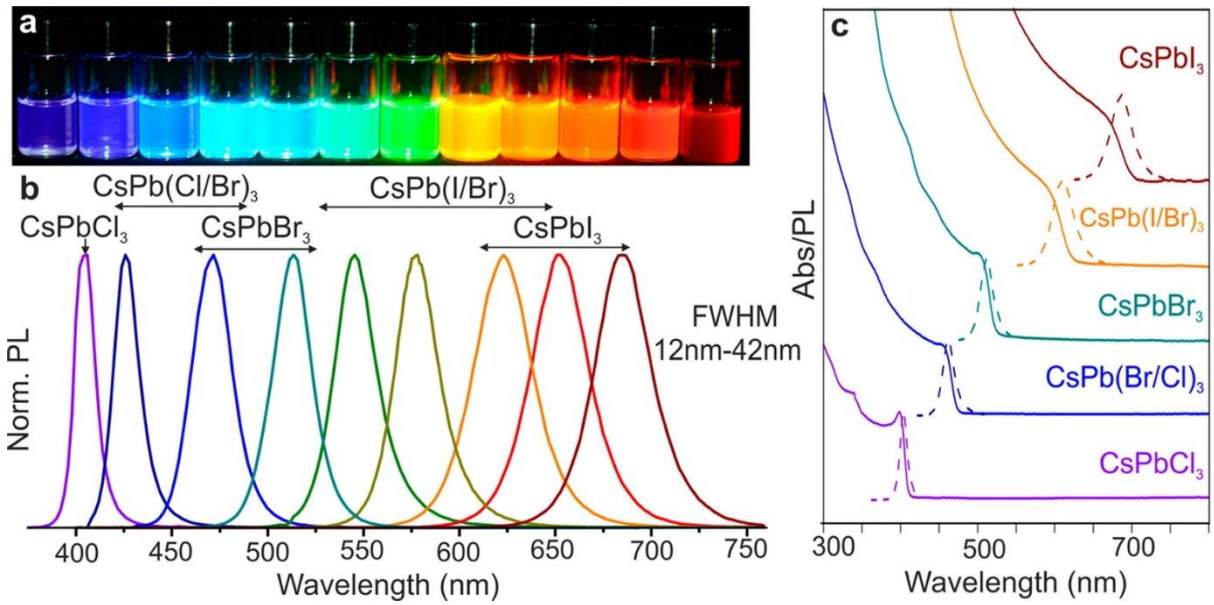

Figure 1.1: Tunable PL spectra of $CsPbX_3$ (X = Br, Cl, I or mixed systems Br/Cl, Br/I) NCs. (a) Colloidal solutions of different compositions of $CsPbX_3$ NCs. (b) Tunability of spectra in the wavelength range 410-700 nm. (c) Absorption and PL spectra of all compositions of $CsPbX_3$ NCs. (Adapted with permission from Protesescu et al.[13] Copyright (2015) American Chemical Society).

Later, Swarnkar et al. showed (i) narrow full width half maximum (FWHM) of 85 meV, (ii) temperature independent chromaticity in the range 25 ^oC till 100 ^oC, (iii) less influence of Förster Resonance Energy Transfer (FRET) and self-absorption on chromaticity, (iv) batch to batch reproducibility for a particular wavelength of 510 nm using $CsPbBr_3$ NCs[14]. It is to be noted that chromaticity is the quality of light with regard to its peak position (wavelength with maximum intensity peak) and spectral width (given by FWHM of the peak).

The properties of $CsPbBr_3$ NCs like narrow FWHM, less impact from FRET (at higher concentrations) have been illustrated in Figure 1.2. Importantly, these $CsPbBr_3$ NCs exhibit suppression in luminescence blinking[14]. Swarnkar et al.[14] has also shown that $CsPbBr_3$ NCs exist in orthorhombic perovskite structure, unlike Protesescu et al.[13] which suggests cubic phase.

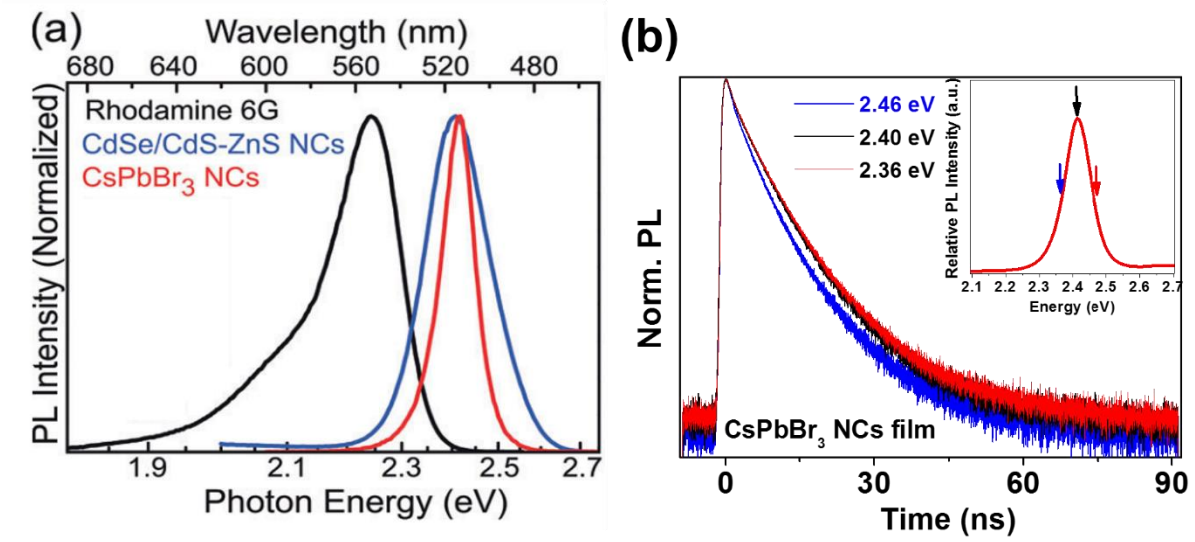

Figure 1.2: (a) Comparison of normalized PL spectra of Rhodamine-6G, CdSe/CdS-ZnS NCs and $CsPbBr_3$ NCs (b) PL decay of $CsPbBr_3$ NC film at different emission energies. Inset shows PL spectrum with color coded arrows to indicate emission energies. (Adapted with permission from Swarnkar et al.[14] Copyright (2015) Wiley Online Library).

Perovskite structures

In general, perovskite structures have a chemical formula, ABX_3 where A and B are two different sized cations and X is an anion. The ideal structure complying with relative sizes of the ions leads to formation of a cubic unit cell which has corner positions occupied by A (0, 0, 0) atoms, body-centers by B (½, ½, ½) atoms and face-centres by C (½, ½, ½) atoms[15]-[18]. In other words, 'perovskites' are comprised of inorganic $[PbX_6]^{4-}$ octahedron and cation A^+ as counter ion. They are made up in such a way that the octahedra share their corners each other and can form networks from zero dimension (0D) to three dimensions (3D)[19]. The ideal arrangement of a perovskite leads to formation of a cubic structure as shown in Figure 1.3 (a), but if the ions do not match the relative size requirements, the cubic structure can get distorted to lower symmetry versions, mainly to orthorhombic (Figure 1.3 (b)) or tetragonal shapes[18].

In the cubic structure the bond angle between B-X-B atoms is found to be 180^{o} whereas in the case of orthorhombic structure it is distorted.

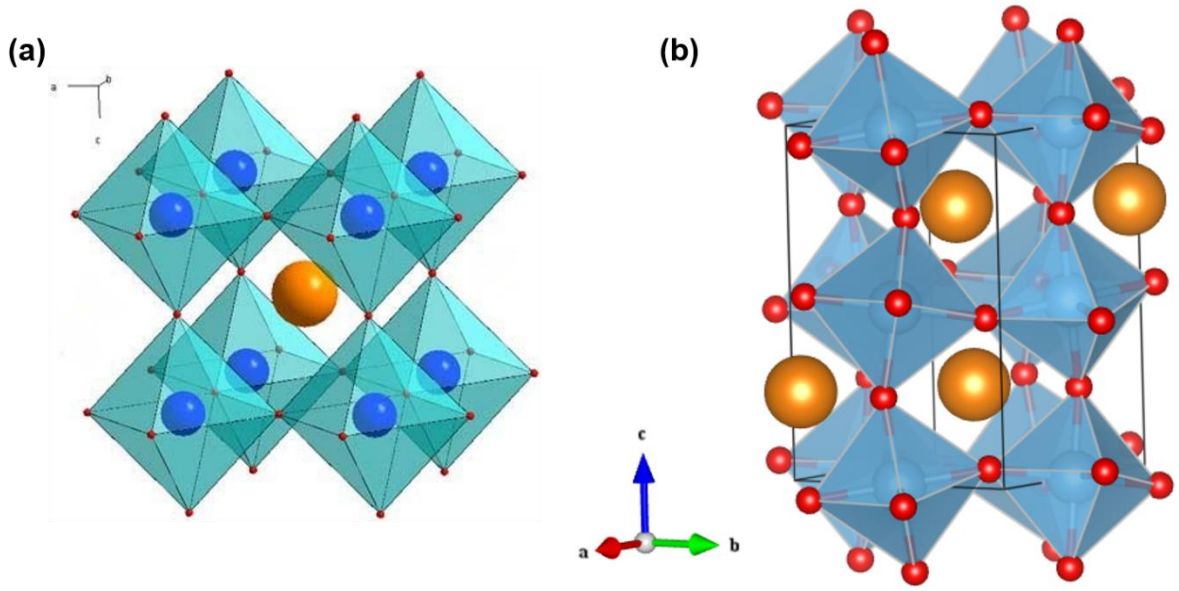

Figure 1.3: (a) Cubic perovskite structure with ABX_3 formula which shows an equivalent cubic unit cell to that explained above and has A (brown) atoms at the body center, B (blue) atoms at the corners of the unit cell and X (red) atoms in the middle of the edges. (b) Orthorhombic perovskite structure that shows that the bond angle between B-X-B atoms is not 180^{o}. (Images adapted from Google Images)[20][21].

$CsPbBr_3$ NCs: Why is it special ?

Traditional quantum dots (QDs) are able to exhibit intense PL only when the charge carriers are strongly confined, which provides a strong overlap of electron and hole wave functions that in turn increases their transition probability. For example CdSe based QDs show high luminescence when their sizes are comparable to 5.6 nm (Bohr-excitonic diameter of CdSe)[20].

QDs are small-sized semiconductor NCs, when the size of the NCs is comparable to the Bohr-excitonic diameter of the bulk material. Therefore, the charge carriers get confined within a QD, which in turn leads to size and shape dependent electronic and optical properties. The band gap of a QD is inversely proportional to the size of the particle, and therefore, the frequency of band-edge PL increases as the size of the QD decreases[23]. So, by adjusting the size of the QD synthesized, we can have a control over its optical and electronic properties.

From the point of view of PL spectral width, the condition of confinement is itself a disadvantage because with confinement, different sizes of NCs emit at different energies. So, the size distribution, which is inevitable even in the state-of-the-art synthesis, can cause PL broadening, reducing the color purity. Thus, in the case of traditional CdSe based QDs, FWHM of PL from an ensemble of NC is significantly broader compared to that of a single NC PL. Here, in the case of ~ 11 nm $CsPbBr_3$ NCs, size distribution does not cause much difficulty as these highly luminescent NCs have sizes greater than the Bohr-excitonic diameter, i.e. they are outside the confinement regime. Consequently, FWHM of single NC PL is comparable to that of PL from NC ensemble. The calculated Bohr-exciton diameter for $CsPbX_3$ (X = Br, Cl, I) perovskites are as follows[13]: $CsPbBr_3$: 7 nm; $CsPbCl_3$: 5 nm; $CsPbI_3$: 12 nm.

Another issue of traditional QDs is FRET and self-absorption. At higher concentrations, when the NCs are close to each other, smaller NCs absorb radiation and when it emits, this radiation is being absorbed by larger NCs (with smaller optical gap). This process is termed as self-absorption. Similarly, at close proximity, the smaller NCs can also transfer its energy non-radiatively to larger NCs. This one is termed as Förster Resonance Energy Transfer (FRET).

So, $CsPbBr_3$ NCs prove to be really advantageous over the traditional CdSe based QDs and with the all above mentioned properties[14] (especially intense PL along with good color purity), they are a potential candidate for Light emitting devices. But since they can emit only a particular energy, their application in display devices gets limited. Hence, tuning the emission wavelength, without losing the above mentioned properties, has to be achieved over the entire visible region[13].

Size dependent tuning of emission wavelengths is not appreciated as when the particle size gets smaller, it goes to QC regime and PL broadening becomes almost inevitable. Another limitation of size-tuning is the bulk band gap of the material, which corresponds to the upper limit of PL emission energy, beyond which the emission wavelength cannot be tuned by varying the size.

Compositional modulation remains the key for tuning the emission energies. $CsPbX_3$ (where X = I, Br/I) can be used to tune the emission spectra to lower energies. But, this work is focused to look at these properties only towards higher energies (lower wavelengths).

Objective of the study

To synthesize $CsPbX_3$ NCs (X = Br, Cl and mixed system Br/Cl) and to tune the emission of $CsPbBr_3$ NCs towards higher energies in the visible spectrum without compromising on the excellent optical properties like high PL QY with narrow FWHM, temperature independent chromaticity, and less influence of FRET and self-absorption in governing the chromaticity of the material.

Chapter-2: Materials and Methods

Experimental Section

Chemicals: Cesium carbonate: Cs_2CO_3 (99.9%, Aldrich), Lead (II) bromide: $PbBr_2$ (99.999%, Aldrich), Lead (II) chloride: $PbCl_2$ (anhydrous, 99.999%, Aldrich), Oleic acid (OA, 90%, Aldrich), Oleylamine (OAm, technical grade 70%, Aldrich), 1-Octadecene (ODE, technical grade 90%, Aldrich), Trioctylphosphine (TOP, 97%, Aldrich), Toluene (99.5%, Rankem), n-butyl alcohol (AR 99.5%, Rankem), Hexane (98%, Chemlabs), Rhodamine-6G (99%, Aldrich), Ethanol (99.9% AR, S D Fine chem. Ltd).

Preparation of Cesium oleate:

Cs_2CO_3 (0.407 gm: 1.25 mmol), ODE (20 ml) and OA (1.25 ml) were added to a 3-neck round bottom (RB) flask. The mixture was dried for 1 hr (under vacuum) at 120 ^oC, with constant magnetic stirring and then N_2 gas was purged in; this process of alternate vacuum and N_2 atm. was done to remove O_2 and moisture from the reaction mixture. It was then heated to 150 ^oC (in N_2 atm.) until all Cs_2CO_3 gets reacted with OA. The reaction was stopped when a clear, transparent solution was obtained. Cs-oleate was pre-heated to 100 ^oC before injection into the reaction mixture since it precipitates out of ODE at room temperature.

Synthesis of colloidal $CsPbX_3$ NCs: Hot Injection method

The synthesis of colloidal $CsPbX_3$ NCs was performed by making some modifications in the synthesis method proposed by Protesescu et al.[13]. 4 ml of ODE was dried (The liquid reagent was taken in an RB and vacuum was applied for one hour at 100 ^oC with constant magnetic stirring) at 110 ^oC (under vacuum) for 1 hr and then cooled down to room temperature in a 50 ml round bottom flask, to which PbX_2 (0.188 mmol) such as $PbBr_2$ (0.069g), $PbCl_2$ (0.052 g) or their mixtures (in 1 ml dry ODE) were added. The reaction mixture was then heated to 120 ^oC (under vacuum) for 1 hour to ensure moisture-free environment. N_2 gas was purged in between (4-5 times) for the removal of O_2 from the system, after which 0.5 ml of dried OAm and OA each were injected into the same (in N_2 atm.) at the same temperature and stirred for ~10 min for their dissolution. $PbCl_2$ doesn't get dissolved in this condition, so 1 ml TOP has to be injected into the mixture after heating to 165 ^oC and stirred vigorously for about 1 hour.

When the mixture becomes clear, the temperature was raise to 190 ^{o}C and 0.4 ml of Cs-oleate (0.125 M, in ODE) (prior heated to 100 ^{o}C) was injected. The reaction was then immediately (within 10-20 sec) quenched using an ice-bath.

Isolation of $CsPbX_3$ NCs:

A 1:1 (v/v) solution was prepared by adding the whole reaction mixture to an equal volume of n-butyl alcohol. Centrifugation (11000 rpm, 6 min) was done to precipitate the sample out. The supernatant was discarded and the precipitate was re-dispersed in toluene. Following this, another centrifugation (3000 rpm, 5 min) was done and the supernatant (colloidally stable) was stored in vials for various characterizations.

Instrumentation

UV-Visible Absorption spectra for both colloidal solution and thin films were collected by Perkin Elmer, Lambda-45 UV/Vis spectrometer. Steady state PL and PL Decay dynamics using time correlated single photon counting (TCSPC) of NCs were measured using FLS 980 (Edinburgh Instruments) for both dispersion and thin film samples. Temperature dependent PL measurements were recorded using TLC 50 temperature controlled cuvette holder for fluorescence (Edinburgh FLS 980). Powder X-ray diffraction (XRD) data were collected using a Bruker D8 Advance x-ray diffractometer using Cu Kα radiation (1.54 Å). Transmission electron microscopy (TEM) studies were carried out using a JEOL JEM 2100 F Field Emission Transmission electron microscope at 200 kV. Energy-dispersive X-ray Spectroscopy (EDAX) data was collected using Zeiss Ultra Plus SEM Instrument.

Origin 8.5 was used for plotting and analysis of all the data given in the report.

Quantum Yield calculation

Room temperature photoluminescence quantum yield of all the $CsPbX_3$ samples were calculated with the help of Rhodamine-6G dissolved in ethanol (with a known quantum yield of 0.96) taken as the reference. The absorbance of Rhodamine-6G (at λ_{max}) and the sample (at first excitonic peak) were adjusted to be at ~0.1 while the spectra were recorded. For a better signal to noise ratio, the absorption scan for Rhodamine-6G was run 5 times and an average of these were taken. The start and stop wavelengths, Bandwidth, Scan speed, Data Interval were all set to be the same for both reference

and the sample. While taking the photoluminescence measurements, PL of Rhodamine-6G was recorded at the same excitation wavelength as that of the sample. Also, PL spectra for Rhodamine-6G was recorded 15 times successively without taking the cuvette out and then averaged out to obtain a better plot for sample comparison. Along with excitation wavelength, Slit widths, Range of X-axis, Dwell time were kept exactly same for both Rhodamine-6G and the sample.

The following equation has been used to calculate the quantum yield of the sample:

$$QY_s = QY_{ref} \cdot \frac{F_s}{F_{ref}} \cdot \frac{A_{ref}(\lambda_{exc})}{A_s(\lambda_{exc})} \cdot \frac{n_s^2}{n_{ref}^2}$$

where:

λ_{exc} = Fixed PL excitation wavelength
QY_s = PL quantum yield of the sample (unknown)
QY_{ref} = PL quantum yield of the reference (known)
F_s = Integrated PL intensity (i.e. area under PL Curve) of the sample (at λ_{exc})
F_{ref} = Integrated PL intensity (i.e. area under PL curve) of the reference (at same λ_{exc})
$A_{ref}(\lambda_{exc})$ = Absorbance value of the reference at λ_{exc}.
$A_s(\lambda_{exc})$ = Absorbance value of the sample at same λ_{exc}.
n_s = Refractive index of the solvent in which sample is dispersed. (Toluene: 1.4969).
n_{ref} = Refractive Index of the solvent in which reference is dispersed.(Ethanol: 1.3614).

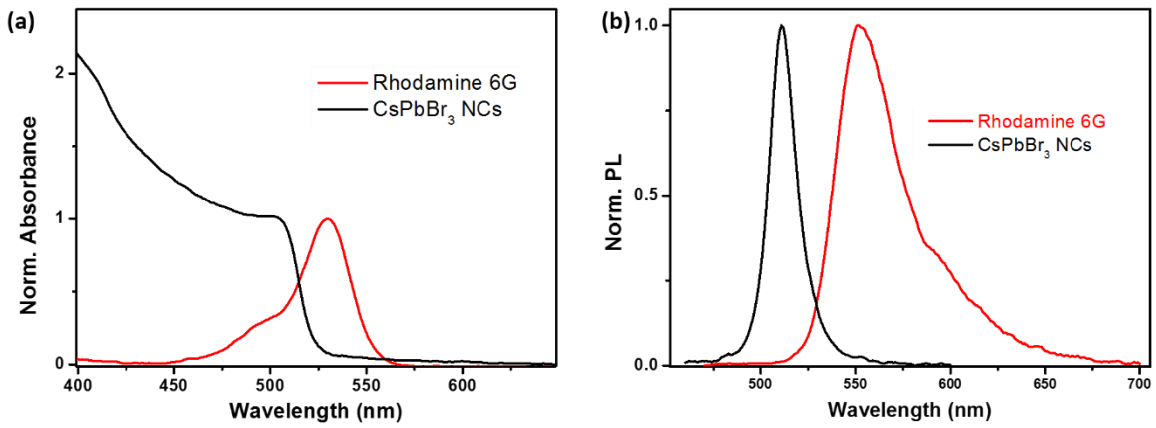

Figure 2.1: Comparison of normalized Absorption and PL spectra of $CsPbBr_3$ NCs and Rhodamine-6G. (a) Shows the Absorbance (normalized at λ_{max} for Rhodamine-6G and at lowest energy excitonic peak for $CsPbBr_3$ NCs) spectra of both Rhodamine-6G and $CsPbBr_3$ NCs (b) shows the normalized PL spectra of both.

For all the quantum yield measurements, the absorption and PL spectra were recorded from the same sample as the PL spectrum has to be absorbance normalized for comparison. Also, it has to be noted that the absorbance at peak position has to be

maintained at ~0.1 for both the reference and the sample to get rid of inner filter effect and also reabsorption which can make the calculation erroneous.

Calculation of molar extinction coefficient

Molar extinction coefficient gives an idea about the capability of light absorption by any material. Here, we try to calculate the molar extinction coefficient (often denoted as ϵ) of $CsPbBr_3$ NCs with the help of Beer Lambert's law where

$$A = \epsilon.C.L$$

A = Absorbance of the sample at the first (least energy) excitonic peak, C = concentration of NCs (in moles/L (M)) and L = path length of light passing through the sample. (Here, 1 cm).

For calculation, dried powder of $CsPbBr_3$ NCs with known weight was dispersed in toluene (of known volume). (Dried weight, here means the weight of only inorganic $CsPbBr_3$ NCs, as Thermogravimetric analysis (TGA) was carried out to get rid of weight of organic capping ligands). This dispersion of $CsPbBr_3$ NCs in toluene is kept as the stock solution. Various amounts of the stock was diluted by adding 3 ml of toluene and their Absorbance v/s concentration plots were recorded. The slope of the linear fit of this plot gives ϵ (in $M^{-1}cm^{-1}$)

Concentration of the NC solution is calculated in the following way: mass of 1 NC is calculated as density × volume (where density of orthorhombic $CsPbBr_3$ = 4.86 g/cm^3 and volume = 11×11×11 nm^3) of 1 NC. Now, the dried weight is divided by mass of 1 NC to obtain the total no. of NCs in the dried sample solution. No. of NCs divided by Avogadro number gives no. of moles of NCs present. Then, the molarity of stock solution is calculated as the no. of moles of NCs divided by volume of NC solution (in litres).

From the molarity of stock solution, molarity of diluted concentrations were calculated and then Absorbance v/s concentration (of the diluted samples) plots were obtained.

Time Correlated Single Photon Counting (TCSPC)

TCSPC is a widely used technique to study the relaxation of molecules or nanocrystals from a higher energy state to a lower energy ground state. So, it basically helps to measure fluorescence lifetimes[24].

Principle: The excitation source is usually a pulsed LASER. A portion of light goes through the sample and the other portion to the "electronics". The fluorescent sample

emits light, which then passes through a monochromator that filters a particular wavelength. The photodetector with intrinsically high gain detects the light and is processed by Constant fraction discriminator (CFD) which gives proper height and shape for the pulses. The reference signal is also passed through CFD to get rid of jitter in timing of the two signals. Then, the signal from the sample reaches the Time-to-amplitude converter (TAC) [in the reverse TAC mode] and activates the circuit. It then starts charging a capacitor; which is stopped by the signal from the “electronics”. This creates a voltage corresponding to time difference in two signals. The amplified TAC output forms an analog pulse. It is then further given to an Analog to digital converter (ADC) that measures the pulse height and the resolution of ADC decides the number of discrete time values. At last, it is passed through Multi-channel analyser (MCA) for data output. Figure 2.2 shows the schematic for the working of TCSPC for an easy understanding[25][26].

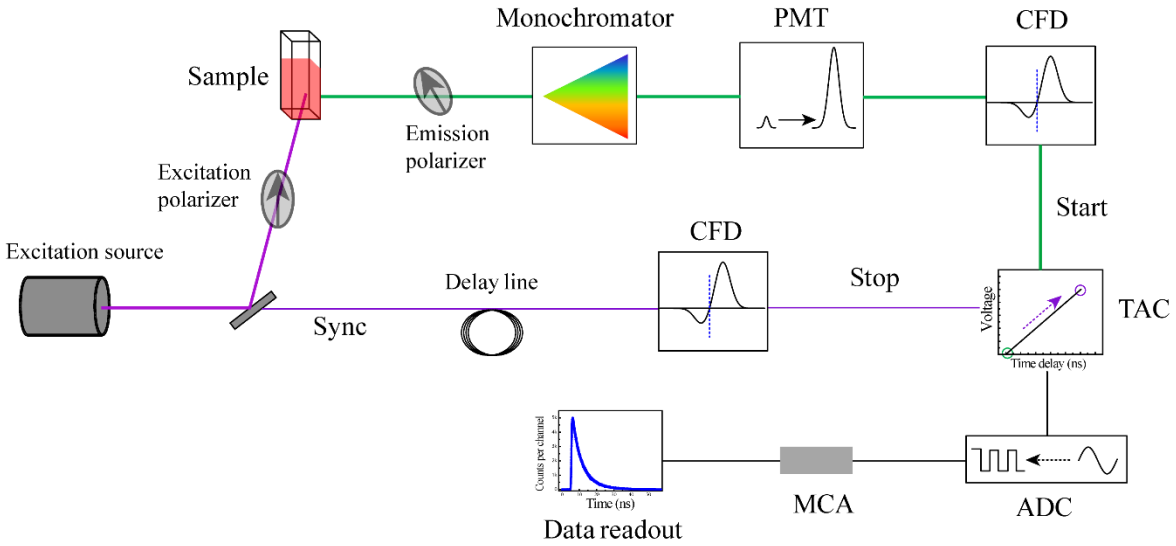

Figure 2.2: Schematic of working of TCSPC (Adapted from [24]).

Chapter – 3: Results and Discussion

Five different compositions of fully inorganic colloidal $CsPbX_3$ (where X = Br, Cl) NCs were synthesized using Hot Injection method[13] namely $CsPbBr_3$, $CsPbBr_{2.7}Cl_{0.3}$, $CsPbBr_2Cl$, $CsPbBrCl_2$, $CsPbCl_3$ NCs and the prepared samples were characterized as follows.

Powder X-Ray Diffraction (XRD)

Powder X-Ray Diffraction (XRD) pattern of all samples were recorded to understand the size and crystal structure of the NCs. The sample for powder XRD measurements was prepared by drop casting a concentrated NC dispersion onto a clean glass slide and was kept for drying for approximately 1 hour under Infrared (IR) lamp and then under vacuum for about 2 hours. The recorded XRD pattern is as shown in Figure 3.1.

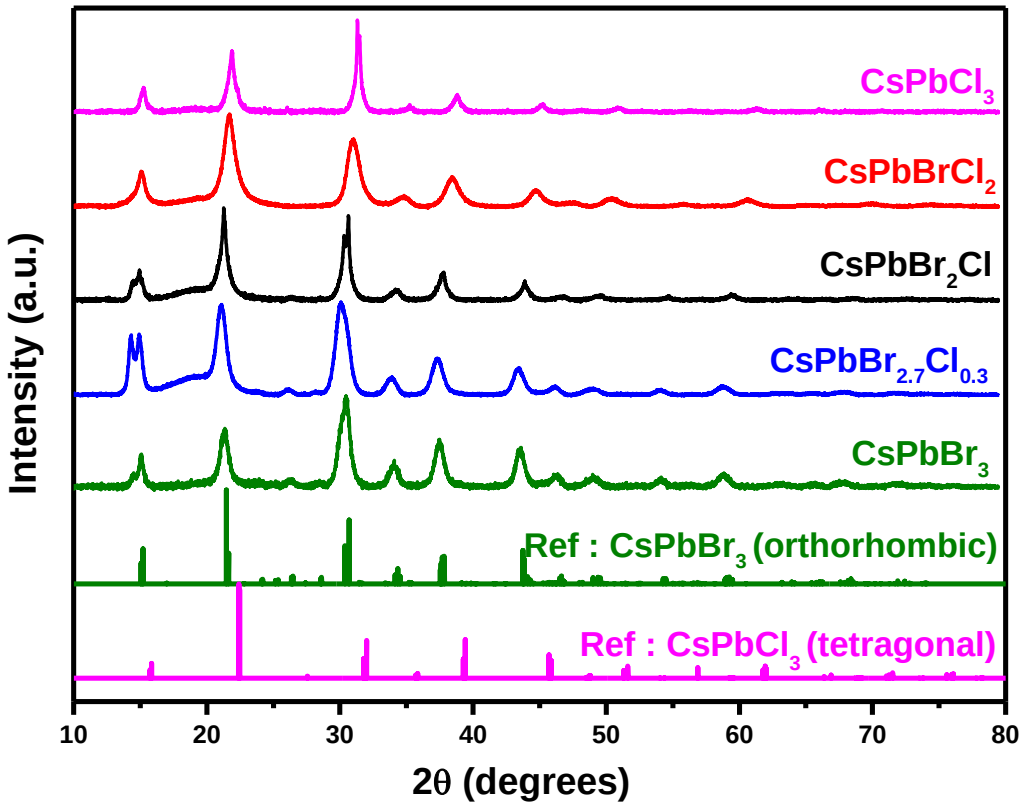

Figure 3.1: XRD patterns of the various compositions of $CsPbX_3$ (X = Br, Cl) NCs, modulating the relative compositions of halides present, along with the reference patterns for bulk $CsPbCl_3$ and $CsPbBr_3$.

XRD pattern suggests that $CsPbBr_3$ NCs are formed in the orthorhombic phase, in agreement with bulk $CsPbBr_3$ (JCPDS No.: 01-072-7929). It is also consistent with reported[27] literature which shows that the most stable phase for $CsPbBr_3$ is orthorhombic phase at room temperature. But the orthorhombic features are not distinct because of (1) the broadening of XRD peaks (due to small sizes of the NCs) and (2) low intensity peaks. The orthorhombic nature of the NCs can still be verified by the presence of less intense peaks in the range of 24^o to 29^o. On the other hand, XRD pattern of $CsPbCl_3$ matches clearly with bulk $CsPbCl_3$ (JCPDS No.: 01-074-6644) in the tetragonal phase, which is again in agreement with the most stable phase for bulk $CsPbCl_3$ reported[28] at room temperature. XRD pattern also illustrates a nice phase transition of $CsPbX_3$ NCs from tetragonal phase to the orthorhombic phase with increase in the bromide composition. The reason could be that, when a bigger ion is being incorporated into the lattice (bromide), it may not be able to meet the ion size requirements for the perovskite structure and gets distorted to lower symmetry orthorhombic structure. This explanation can be validated by using another example, namely $CsPbI_3$ (has a bigger ion), which is most stable at room temperature in its orthorhombic structure (low symmetry). It also indicates that as the bromide composition in $CsPbX_3$ NCs increases, the XRD peaks gets shifted towards lower angles (2θ values) of diffraction. This is expected as when a larger ion gets incorporated, the lattice parameters increases which increases the d-spacing leading to shift in angles towards lower Bragg angles. This could be explained using Bragg's law of diffraction;

$$n\lambda = 2d\sin\theta$$

where n = order of diffraction

λ = wavelength of incident X-ray

d = d-spacing between atomic layers

θ = scattering angle

As d increases, θ decreases, which means the peaks get shifted to lower angles.

Once the crystal structure is obtained, the next obvious step is to know the elements present in it and to see if our expected composition (from precursor ratio) of elements is being achieved or not.

Energy Dispersive X-ray Spectroscopy (EDAX) Analysis

The elemental analysis for all compositions of $CsPbX_3$ (X = Br, Cl) was carried out using EDAX technique. In EDAX, a high energy beam of electrons is being focused onto the sample which excites the core electrons to higher energy states, and higher energy level electrons fill the created holes. This leads to the emission of X-rays with energies corresponding to difference of two energy levels. The number and energy of the X-rays are a characteristic of atomic structure of each element[29].

Samples for EDAX measurements were prepared by precipitation of NCs dispersed in toluene with the help of non-solvents like n-butyl alcohol, acetone etc. The powder obtained was dried under vacuum for 8-10 hrs. Later, a small amount of the powder was taken and stuck onto a carbon tape for EDAX measurements.

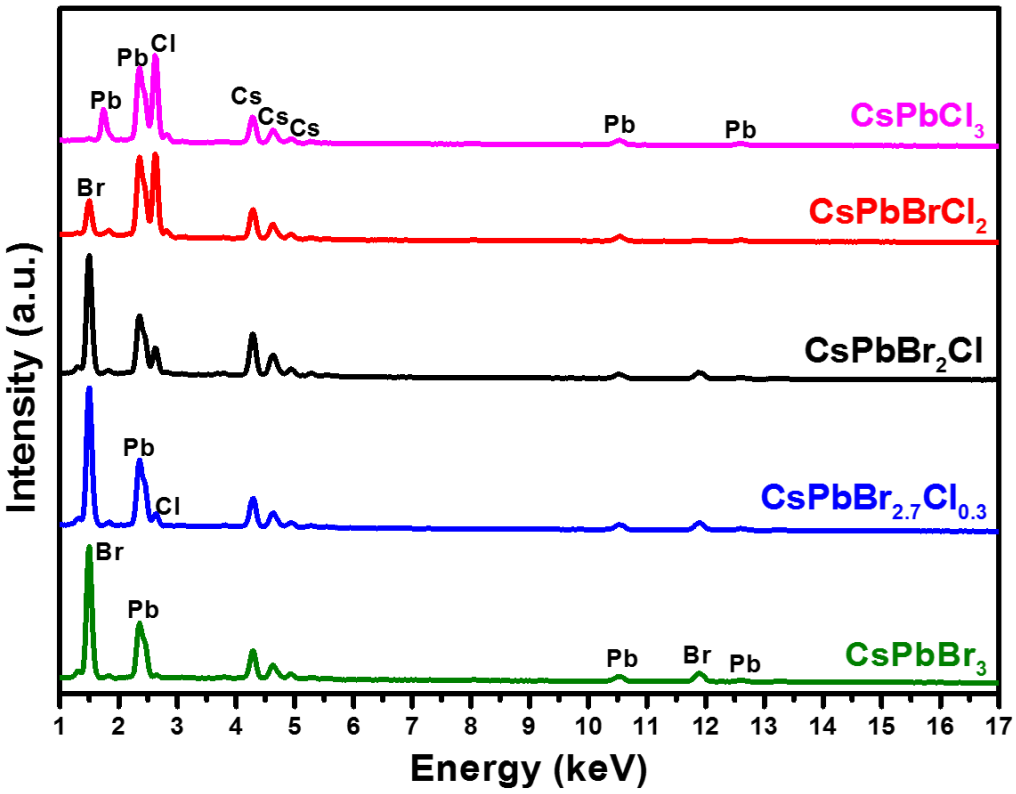

Figure 3.2: EDAX analysis for all the compositions of $CsPbX_3$ NCs. It shows the relative abundance of each atom in the composition.

EDAX Analysis shows that the expected compositions of $CsPbX_3$ (X = Br, Cl, Br/Cl) NCs have been synthesized (Figure 3.2 and Table 3.1). Henceforth, for all the further characterizations and measurements, the precursor ratios would be adopted.

Molecular formula (from precursors)	Molecular formula (from EDAX Analysis)
$CsPbBr_3$	$CsPbBr_{3.4}$
$CsPbBr_{2.7}Cl_{0.3}$	$CsPbBr_{2.8}Cl_{0.4}$
$CsPbBr_2Cl$	$Cs_{1.4}PbBr_{2.9}Cl_{1.1}$
$CsPbBrCl_2$	$Cs_{1.1}PbBr_{0.7}Cl_{2.9}$
$CsPbCl_3$	$Cs_{1.1}PbCl_{3.6}$

Table 3.1: Comparison of the molecular formula expected from the precursor ratios and the molecular formulas deduced from EDAX analysis.

EDAX Analysis also suggest that all the samples prepared show a slight anion excess. The reason behind this could be that the capping ligands are present in the quaternary ammonium cation form. So, the ions at the surface of the NCs become predominantly anionic. But, further studies have to be done to verify the same.

Different compositions of $CsPbX_3$ (X = Br/Cl) NCs as shown in Table 3.1 have been synthesized with the objective of tuning the emission wavelength in the visible spectrum. So, the compositions to be synthesized were chosen accordingly. Also, getting an efficient (good QY) blue emission was one of our motive and $CsPbBr_2Cl$ NCs turned out to be a representative sample for the same.

Transmission Electron Microscopy (TEM)

Now, after obtaining the expected composition, we characterized the morphology of the samples. TEM images were captured to obtain the shape and size of the NCs. The sample preparation was done by putting one or two drops of dilute colloidal NC solution in hexane onto carbon coated copper grids.

The TEM image for colloidal $CsPbBr_3$ NCs having an average edge length of 11 nm is as shown in the Figure 3.3 (a) (Adapted from [14]). Also, the TEM image of $CsPbBr_{2.7}Cl_{0.3}$ NCs (Figure 3.3 (b)) clearly suggests that they form nanocubes with a nice shape and size homogeneity. The mean edge length was found out to be 11 nm. The TEM images of the other two NC compositions namely $CsPbBr_2Cl$ and $CsPbBrCl_2$ are also shown along with. Both of them suggest that they are nanocubes but they do

not show a great shape and size homogeneity. The mean edge length of $CsPbBr_2Cl$ NCs was found out to be 14 nm whereas of $CsPbBrCl_2$ was 12 nm. From the sizes of the NCs obtained, it is clearly seen that none of them lies in the QC regime which automatically eliminate to an extent the size distribution problem. The inhomogeneity in the last two samples could be because of more washing with non-solvent. Because more washing might take off some of the capping ligands which can lead to agglomeration of the NCs and formation of a size distribution.

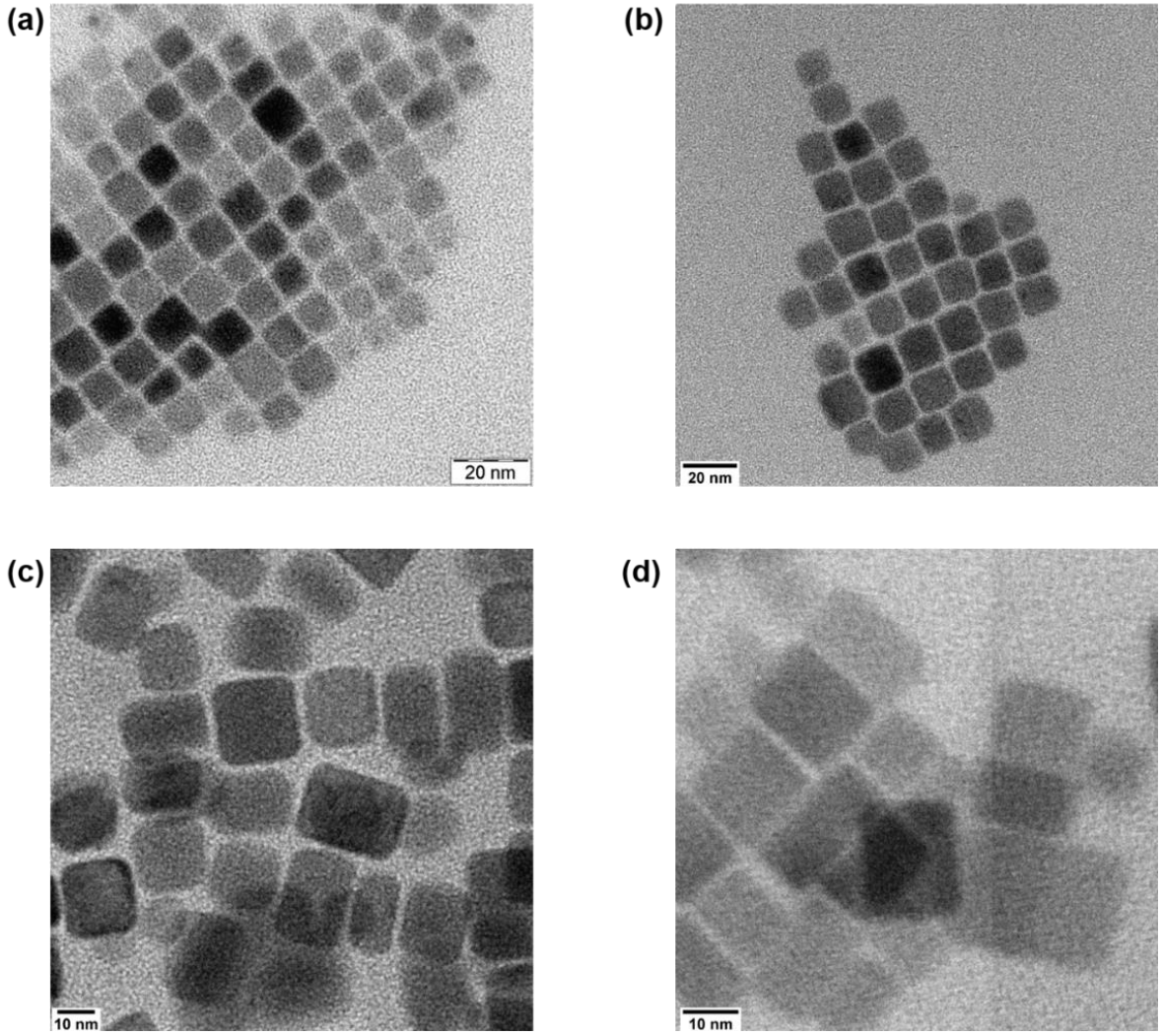

Figure 3.3: (a)-(d) TEM images for different compositions of $CsPbX_3$ NCs. TEM images of (a) $CsPbBr_3$ NCs (Adapted from [14]) (b) $CsPbBr_{2.7}Cl_{0.3}$ NCs (c) $CsPbBr_2Cl$ NCs and (d) $CsPbBrCl_2$ NCs.

Having obtained the crystal structure, elemental composition, size and shape of the NCs, it's been verified that different compositions of $CsPbX_3$ (X = Br, Cl) NCs have formed properly. Then, the investigation on optical properties had to be carried out.

Optical measurements

Absorption and photoluminescence (PL) spectra of all the five different compositions of colloidally stable $CsPbX_3$ (X = Br, Cl) NCs are shown in Figure 3.4. For all the optical measurements, the nanocrystals were dispersed in toluene and air-tight screwcap cuvettes were used. Also, all the measurements, other than the temperature dependent studies were carried out at room temperature. The absorption and PL spectra plotted together shows the band edge emission of $CsPbX_3$ (X = Br, Cl, Br/Cl) NCs. Here, the spectra are stacked one on top of other just for easy comparison.

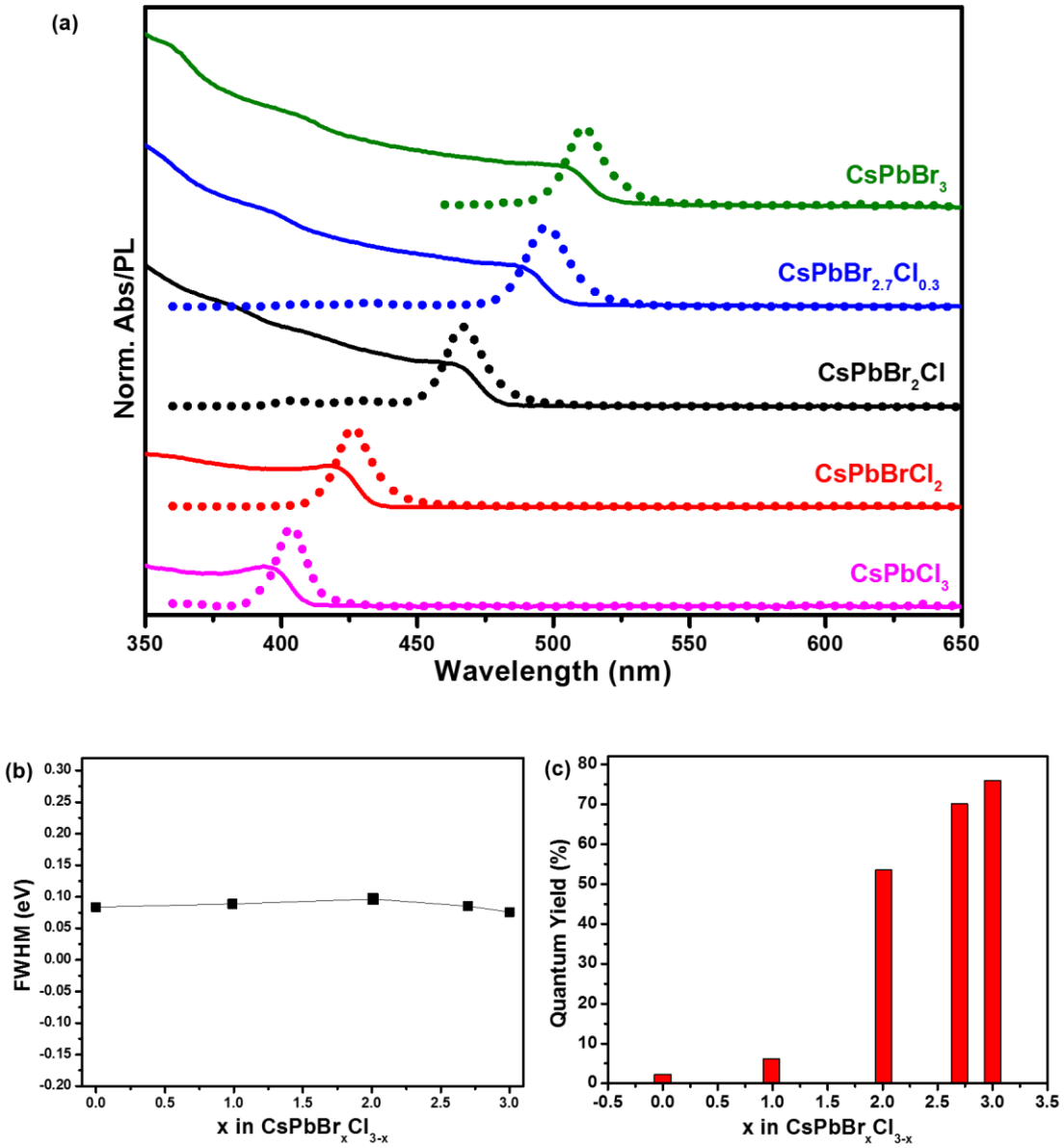

Figure 3.4: UV-Vis absorption, PL, FWHM and QY plots for all compositions (a) Plot of both PL (dotted lines) and absorption (solid lines) spectra for all compositions. (b) FWHM for all compositions plotted together against x in $CsPbBr_xCl_{3-x}$. (c) QY of all compositions plotted together.

The absorption and PL spectra as shown in Figure 3.4 (a) demonstrate that the tuning of the spectra in the wavelength regime of 400-515 nm was achieved with narrow FWHM (75-95 meV) (Figure 3.4 (b)) for all the compositions. Also $CsPbX_3$ (X = Br, Cl, Br/Cl) NCs show good quantum yield when x in $CsPbBr_xCl_{3-x}$ is greater than or equal to 2 (i.e. when the bromide composition is greater than 65% with respect to the chloride composition) (Figure 3.4 (c)). Figure 3.4 (a) also shows that band gap increases as the chloride composition in $CsPbX_3$ (X = Br, Cl, Br/Cl) NCs increases.

The reason for tuning the band gap by changing the composition of X is explained in the following manner: Molecular orbitals are formed by the interaction between atomic orbitals of cation and anion. Different anions have different valence orbital energies. So, when the anion in the NC changes, their interaction with the cation valence energy level changes. The molecular orbitals formed can have different stabilizations and so the gap between the bands formed by these molecular orbitals also changes. The absorption and emission spectra of $CsPbX_3$ NCs is tuned by changing the composition of X in a similar way. High QY is observed by $CsPbX_3$ NCs emitting in wavelength range 465 – 515 nm which says there is less probability of defects present in the gap present between Valence band maximum (VBM) and Conduction band minimum (CBM). This is because of their unique electronic structure which will be explained in the later section.

Narrow FWHM (Figure 3.4 (b)) is obtained for all samples. The size distribution does not broaden the PL spectra in the case of $CsPbX_3$ (X = Br, Cl, Br/Cl) NCs as the average size of the NCs is more than the Bohr-excitonic diameter and so, lies outside the confinement regime. This implies that the optical gap is independent of the size of NCs. So, even if distribution of sizes are present, it does not cause PL broadening and we can obtain tunable emission with good color purity.

But by looking at the trend of FWHM from Figure 3.4 (b), it is clear that the FWHM is minimum at the ends ($CsPbCl_3$ and $CsPbBr_3$), so we can say that they have the smallest distribution of compositions whereas for $CsPbBr_2Cl$ NCs they have a bigger distribution of compositions present (like $CsPbBr_{1.99}Cl_{1.01}$ or $CsPbBr_{2.01}Cl_{0.99}$) intrinsically and so, they have more spectral width. But still, all the compositions have less FWHM (less than 100 meV) and PL broadening is less as compared to the traditional QDs exhibiting high QY.

A good PL spectra with narrow spectral width is obtained for $CsPbX_3$ NCs. But it's not yet confirmed if the PL is arising from the NCs or not. To confirm that, we need to do Photoluminescence Excitation (PLE). So, PLE spectra was taken to see the range of excitation wavelengths that can be provided to obtain the particular PL spectrum. In PLE, the excitation wavelengths are varied and luminescence at a particular emission wavelength is monitored[30].

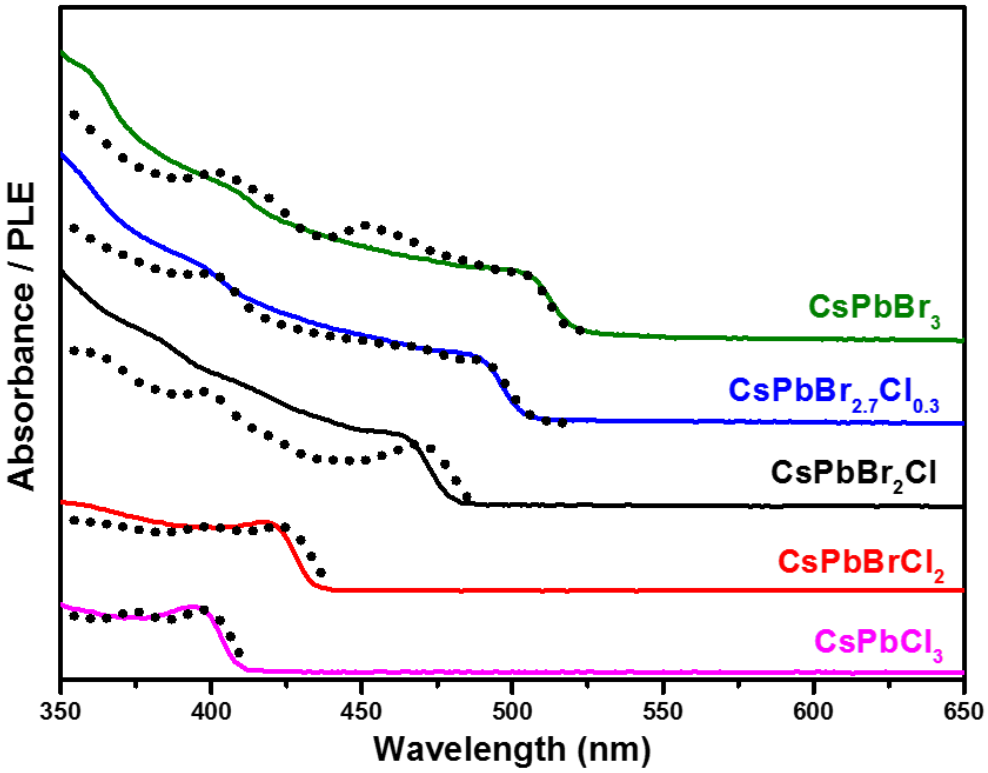

Figure 3.5: PLE plots (black dotted lines) for all compositions of $CsPbX_3$ (X = Br,Cl) NCs and its comparison with the absorption (solid lines) spectra.

The PLE spectra obtained was similar to the absorption spectra obtained as shown in Figure 3.5. This shows that that the luminescence exhibited at that particular region was indeed due to the light absorbed by $CsPbX_3$ NCs.

The emission properties of $CsPbX_3$ NCs show that they exhibit a good PL spectra with high QY (55-80%) in the wavelength range 465 nm to 515 nm. This can only be effective if the NCs have a good absorption probability (or absorption cross-section). Suppose the $CsPbX_3$ NCs have a poor absorption cross-section. Then even if it has high QY, the emission would be less as compared to the amount of light given for excitation, as they absorb very less and only a fraction of this absorbed light can be emitted. So, Molar extinction coefficient (ϵ) can be calculated as its measure. But molar

extinction coefficient of only $CsPbBr_3$ could be calculated as density and size of the NCs are required for its calculation.

Then, ϵ of $CsPbBr_3$ was obtained for the least energy excitonic absorption. It was determined at the lowest energy excitonic peak so as to make sure that the higher energy contribution from capping ligands (organic) on the NC surface does not come up. The absorption spectra of $CsPbBr_3$ NCs at various concentrations and the plot of Absorption v/s concentration are as shown below (Figure 3.6 (a)).

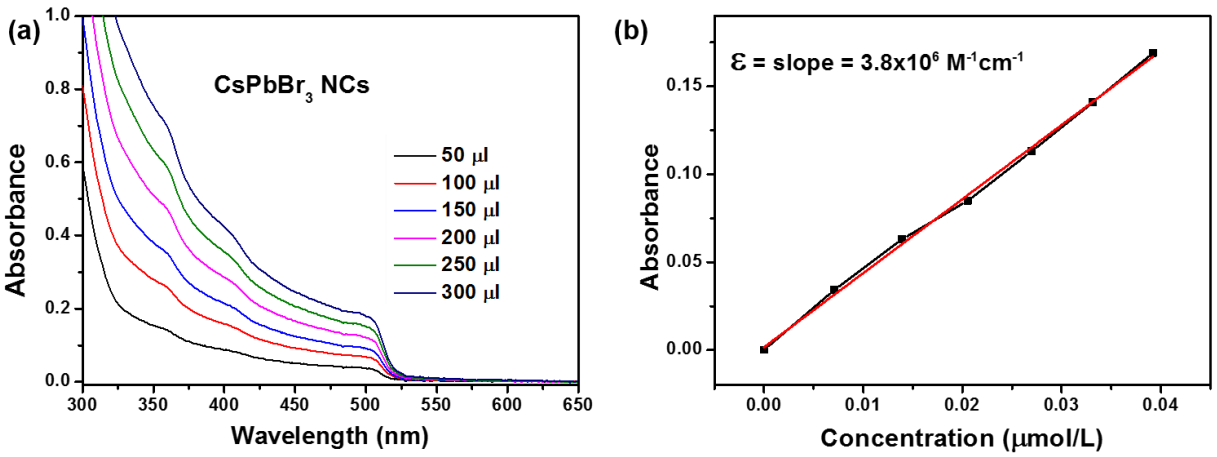

Figure 3.6: Calculation of molar extinction coefficient of $CsPbBr_3$ NCs. (a) show the absorption spectra varying with the concentration and (b) shows the calculated molar extinction coefficient of $CsPbBr_3$ NCs.

The molar extinction coefficient for $CsPbBr_3$ NCs was found to be ~3.8×10^6 $M^{-1}cm^{-1}$. Now, as the molar extinction coefficient is calculated, one can easily find out the concentration of a NC solution, simply by measuring the absorbance and correlating to concentration using Beer-Lambert's law.

Along with that, absorption spectra for all the compositions of $CsPbX_3$ NCs at various concentrations were taken and have seen that they follow Beer-Lambert's law as the absorbance v/s concentration plot gave a straight line. But this data was not used to calculate the molar extinction coefficient of the respective NCs because of the size and shape inhomogeneity. Various plots of Absorbance v/s wavelength and Absorbance v/s concentration were recorded as shown below in Figure 3.7.

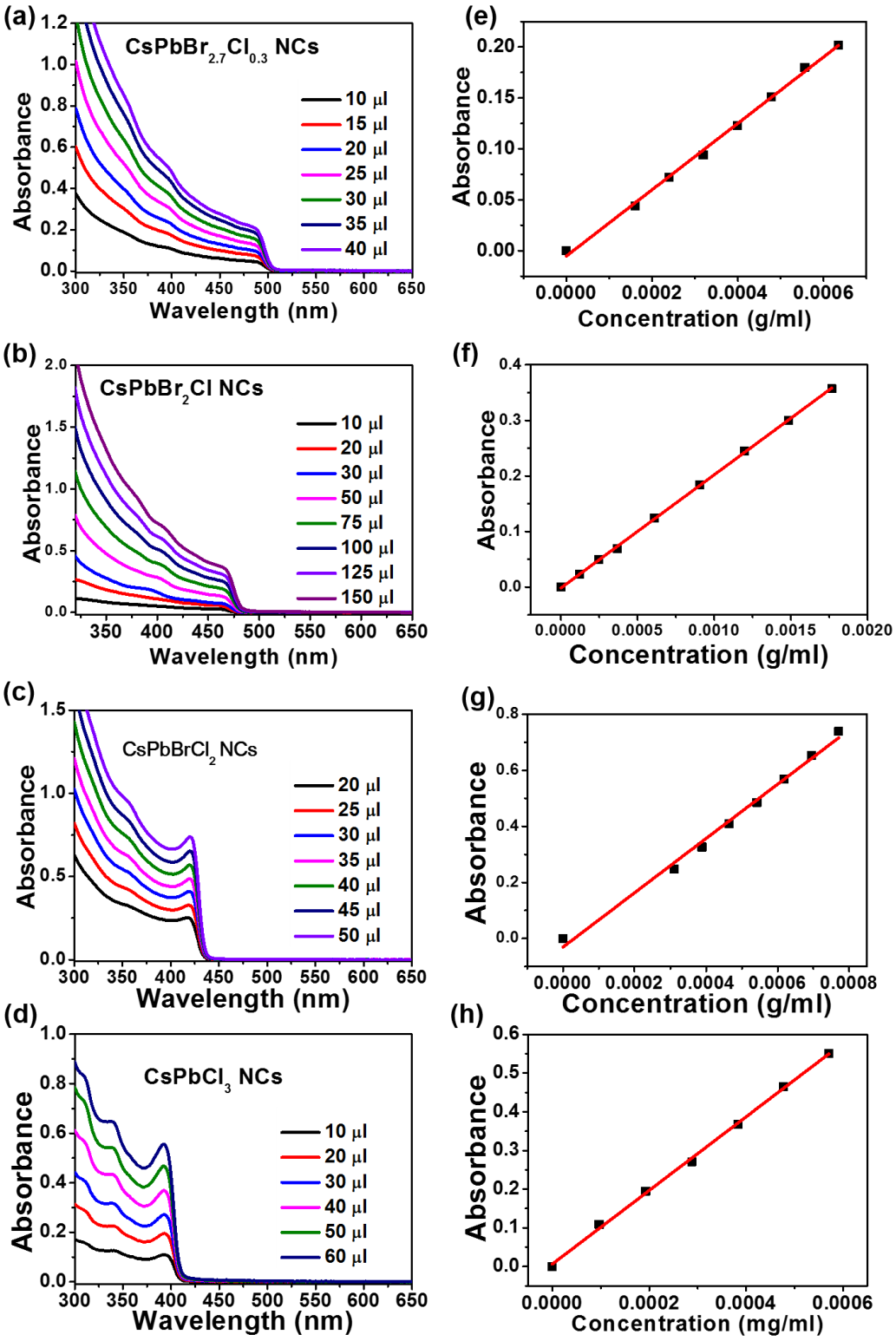

Figure 3.7: (a)-(d) Absorption spectra at various concentrations and (e)-(h) Absorbance v/s concentration plots, for all compositions of $CsPbX_3$ NCs. Absorption spectra for (a) $CsPbBr_{2.7}Cl_{0.3}$, (b) $CsPbBr_2Cl$, (c) $CsPbBrCl_2$ and (d) $CsPbCl_3$ NCs at different concentrations and Absorbance v/s concentration plot for (e) $CsPbBr_{2.7}Cl_{0.3}$, (f) $CsPbBr_2Cl$, (g) $CsPbBrCl_2$ and (h) $CsPbCl_3$ NCs.

The lowest energy excitonic peaks in the chloride rich samples is narrower as compared to bromide rich samples. The calculated optical dielectric constants for $CsPbBr_3$ and $CsPbCl_3$ are 4.96 and 4.07 respectively[13]. Because of the coulombic interaction between the electron and the hole, the exciton binding energy is inversely proportional to the dielectric constant of the material. Thus as the dielectric constant is less for $CsPbCl_3$ as compared to $CsPbBr_3$, the excitonic binding energy will be high for $CsPbCl_3$ and this matches with the calculated exciton binding energies, which are found out to be 75 meV and 40 meV for $CsPbCl_3$ and $CsPbBr_3$ respectively[13]. As the exciton binding energy is higher for $CsPbCl_3$, or rather the Cl-rich samples, the first excitonic peak becomes narrower than $CsPbBr_3$ at room temperature as shown in Figure 3.7.

Another aspect to look at is the chromaticity of the material and its dependence on temperature and concentration of the NCs. To study the temperature dependence on chromaticity, PL measurements were conducted from 20 ^oC till 80 ^oC keeping a step size of 10 ^oC using a temperature-controlled cuvette holder attached to a digital controller. The cuvette holder is a thermoelectric-temperature controlled, 4-window holder with variable speed magnetic stirring and dry gas purge is provided on four windows of the cuvette[31]. For all the measurements, anhydrous toluene was used as the solvent. The following plots were taken to study temperature dependent PL as shown below (Figure 3.8).

As shown in the figure below, with increase in temperature from 20 ^oC to 80 ^oC, colloidal $CsPbX_3$ (X = Br, Cl, Br/Cl) NCs show an anomalous behavior with the shift in peak position as described below: $CsPbBr_3$ NCs gets blue shifted by 2 nm as it reaches 80 ^oC. In the case of $CsPbBr_{2.7}Cl_{0.3}$ NCs also, they show a blue shift, but to an extent of 3 nm when the temperature reaches 80 ^oC. Similarly, $CsPbBr_2Cl$ NCs clearly shows a blue shift of 2 nm when the temperature was increased from 20 ^oC to 80 ^oC. But, $CsPbBrCl_2$ and $CsPbCl_3$ NCs show no change in peak position with increase in temperature in the above mentioned range.

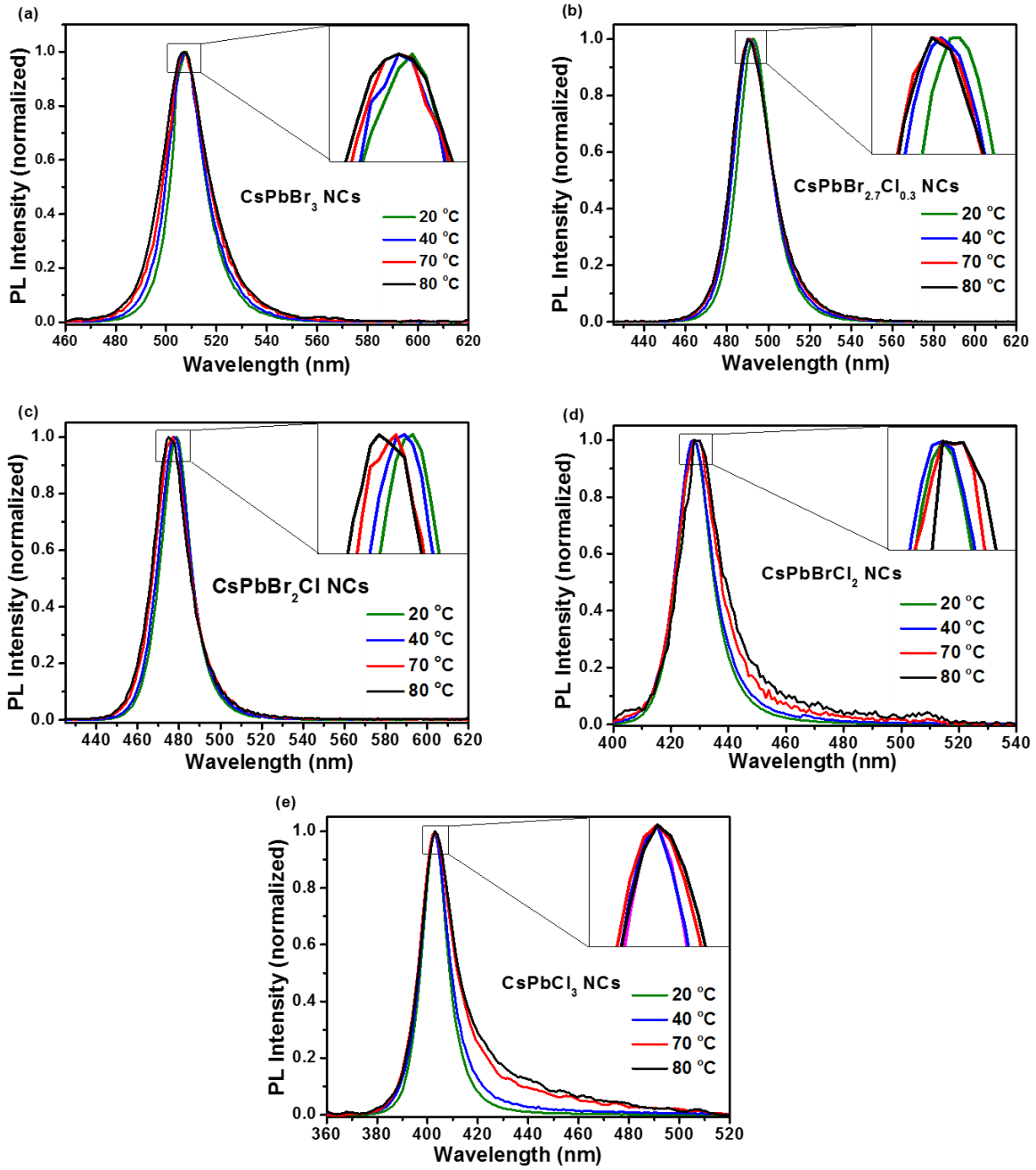

Figure 3.8: Temperature dependent PL plots for various compositions. It shows variation of normalized PL spectrum of (a) $CsPbBr_3$, (b) $CsPbBr_{2.7}Cl_{0.3}$, (c) $CsPbBr_2Cl$, (d) $CsPbBrCl_2$ (e) $CsPbCl_3$ NCs with temperature from 20 ^oC to 80 ^oC. Insets show the magnified view of the shown area to visualize the shift in peak position.

The above trend is being called “anomalous” because the optical gap decreases as the temperature increases for a semiconductor[32]. A red-shift of about 8-9 nm is expected for CdSe and CdSe/CdS-ZnS NCs[14]. Considering the magnitude (of 2-3 nm) of shift, one can observe that its influence on chromaticity is less as compared to

the traditional CdSe based QDs. The unnatural behaviour of $CsPbX_3$ NCs with temperature can be associated with the electronic structure (would be explained in detail later in next section) difference of these type of NCs, where CBM is composed mostly of Pb *p* states and VBM by a mixture of X *p* and Pb *s* states. Due to this, the optical gap transition is mostly intra-atomic between Pb *s* and Pb *p* states[33][11]. So, the lattice expansion that take place due to increase in temperature which, in turn reduces the cation-anion interaction does not affect the optical gap. Also, the blue shift with respect to increase in temperature can be explained as: Due to lattice expansion and decrease in cation-anion interaction, the valence band (VB) width decreases and it leads to slight increase in the gap between CBM and VBM[33]. Also, the decrease in cation-anion interaction does not affect conduction band (CB) as it is composed of Pb *p* states and so, the decrease in cation-anion interaction does not affect the CB. So, as the change is happening only for VB, the magnitude of shift is less. In the case of Cl-rich samples, an inhomogeneous PL broadening is observed for which the reason has to be found out yet. However, it should be noted that for these samples at higher temperature, the intensity is very less which reduces the signal to noise ratio and makes it less reliable for making an inference on PL broadening.

To look at the concentration dependence on the chromaticity, we prepared thin films of $CsPbX_3$ (X = Br, Cl, Br/Cl) NCs. Thin films were prepared by drop-casting the colloidal solution (in toluene) on top of a quartz substrate and then kept for drying under IR lamp for about 1 hour. They were then seen under UV lamp (long UV: 365 nm) to make sure that the film formed is thin enough to transmit the light from the source after absorption.

PL emission spectra of both colloidally stable dispersion and close-packed thin films (having more concentration of NCs) of $CsPbX_3$ NCs were collected and is as shown in Figure 3.9. A red-shift of about 9-10 nm is expected for CdSe and CdSe/CdS-ZnS NCs[14] when thin films were prepared whereas in our case, $CsPbBr_3$ NCs gets blue shifted by 1 nm when drop-casted into thin films. In the case of $CsPbBr_{2.7}Cl_{0.3}$ and $CsPbBr_2Cl$ NCs, they show a blue shift of 2 nm. Also, $CsPbBrCl_2$ NCs showed no change in peak position and $CsPbCl_3$ NCs got red shifted by 1 nm when thin films were prepared as shown below in Figure 3.9. The slight shift happening in every case is not systematic as no trend could be deduced from it. This indicates that when thin films were prepared, no systematic and significant shift in peak position was observed with

negligible increase in PL broadening with respect to the solution dispersed samples for all the compositions of $CsPbX_3$ NCs. So, the shift happening lies within the accepted range of experimental uncertainities.

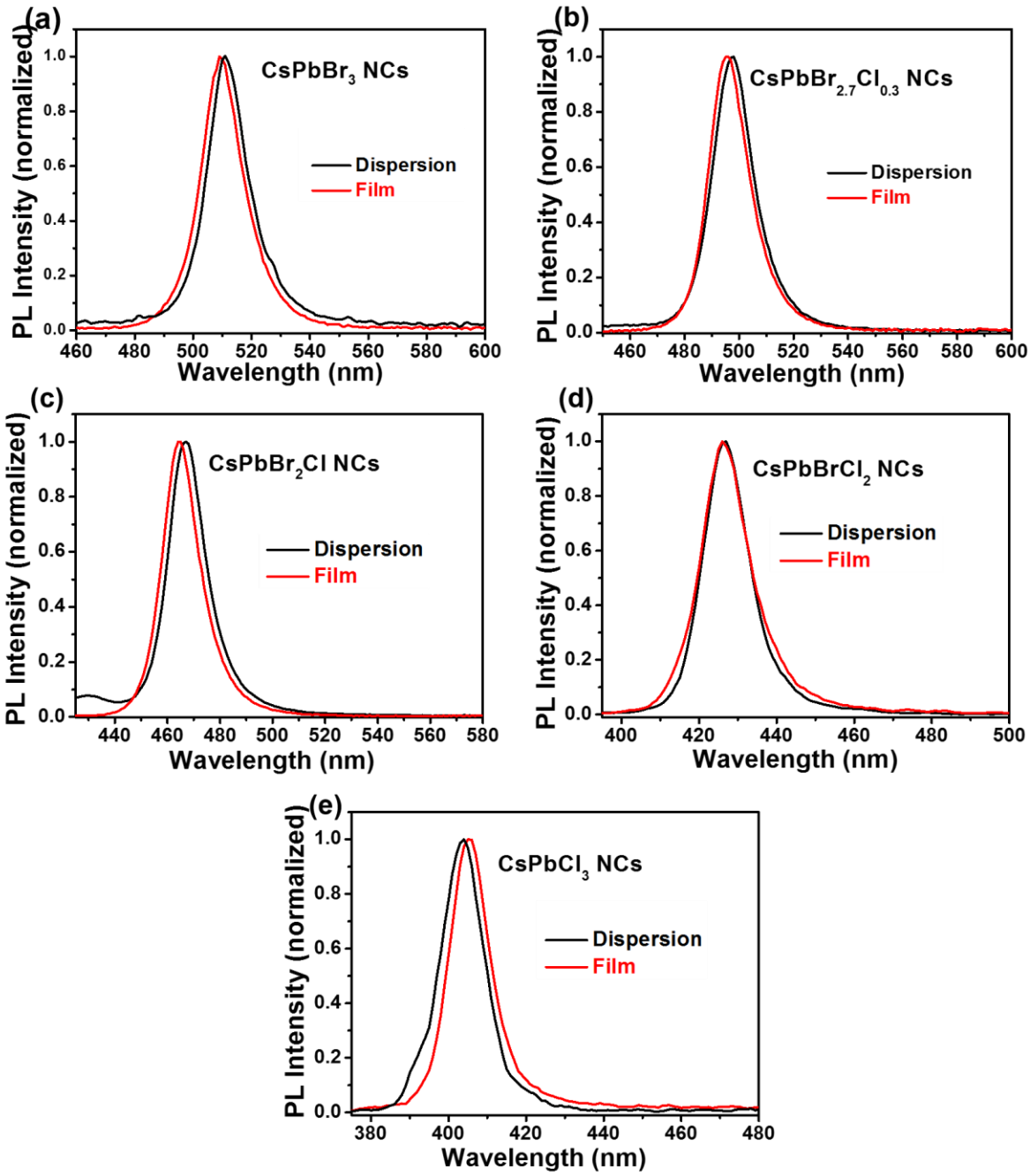

Figure 3.9: PL spectra of solution and film samples for all compositions of $CsPbX_3$ NCs. It shows comparison of PL spectra of dispersion (NC solution in toluene) and thin film samples of (a) $CsPbBr_3$, (b) $CsPbBr_{2.7}Cl_{0.3}$, (c) $CsPbBr_2Cl$, (d) $CsPbBrCl_2$ (e) $CsPbCl_3$ NCs.

This indicates that the color and color purity present in the solution is retained in the films for all the compositions of $CsPbX_3$ NCs which means that at higher concentrations, less self-absorption occurs and has a less impact on the chromaticity. So to an extent, it shows concentration independent chromaticity.

PL decay dynamics of $CsPbX_3$ (X = Br, Cl, Br/Cl) NCs was studied using TCSPC technique. The decay pattern of close-packed thin films (Figure 3.10) and dispersion (solution) samples (Figure 3.11) show similar PL decay at all emission energies as shown below.

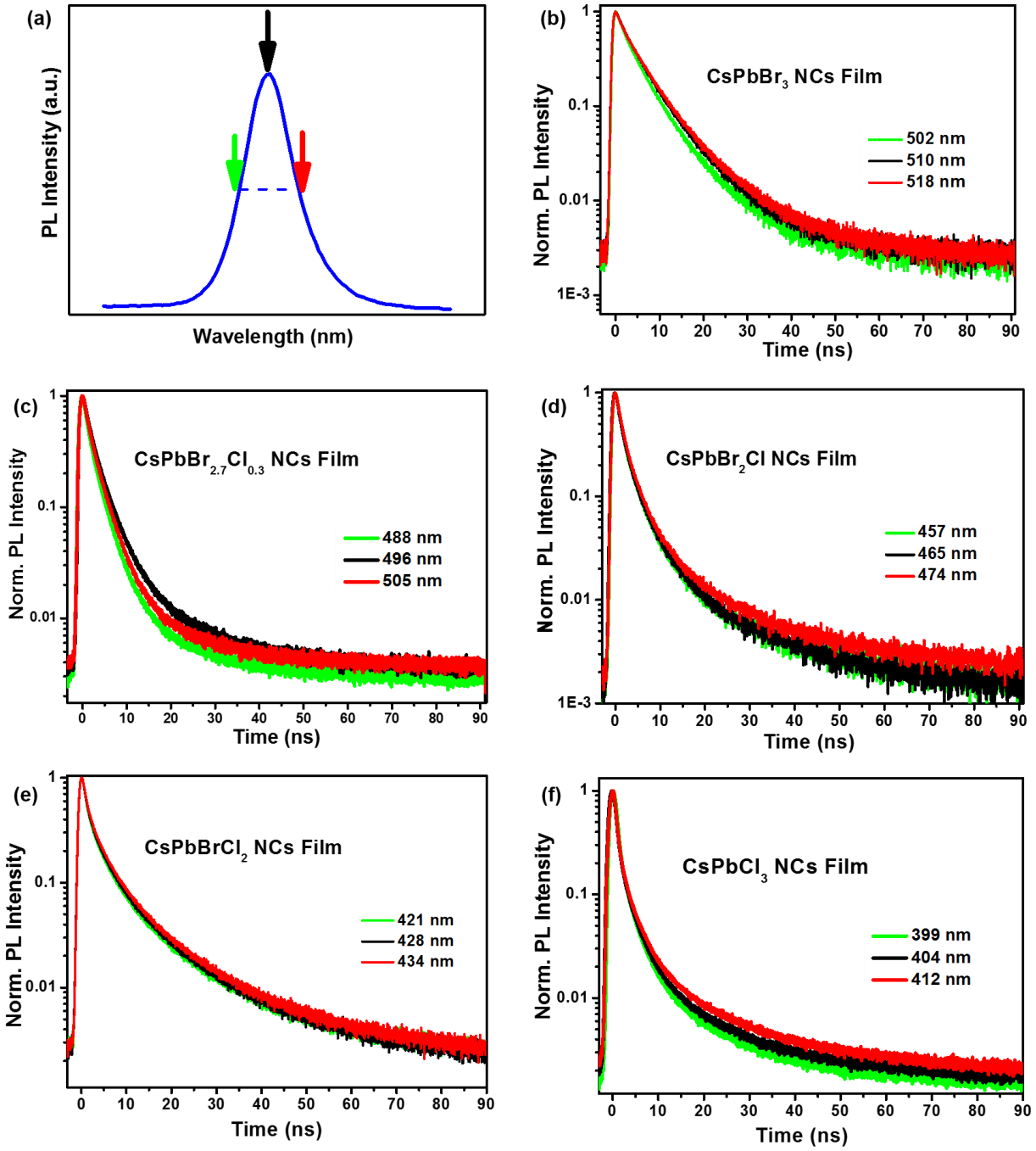

Figure 3.10: PL decay plots for various compositions of $CsPbX_3$ NC films. (a) A representative PL spectrum and the arrows represent the emission energies at which decay is monitored. (b)-(f) PL decay plots for films of (b) $CsPbBr_3$, (c) $CsPbBr_{2.7}Cl_{0.3}$, (d) $CsPbBr_2Cl$, (e) $CsPbBrCl_2$ and (f) $CsPbCl_3$ NCs respectively.

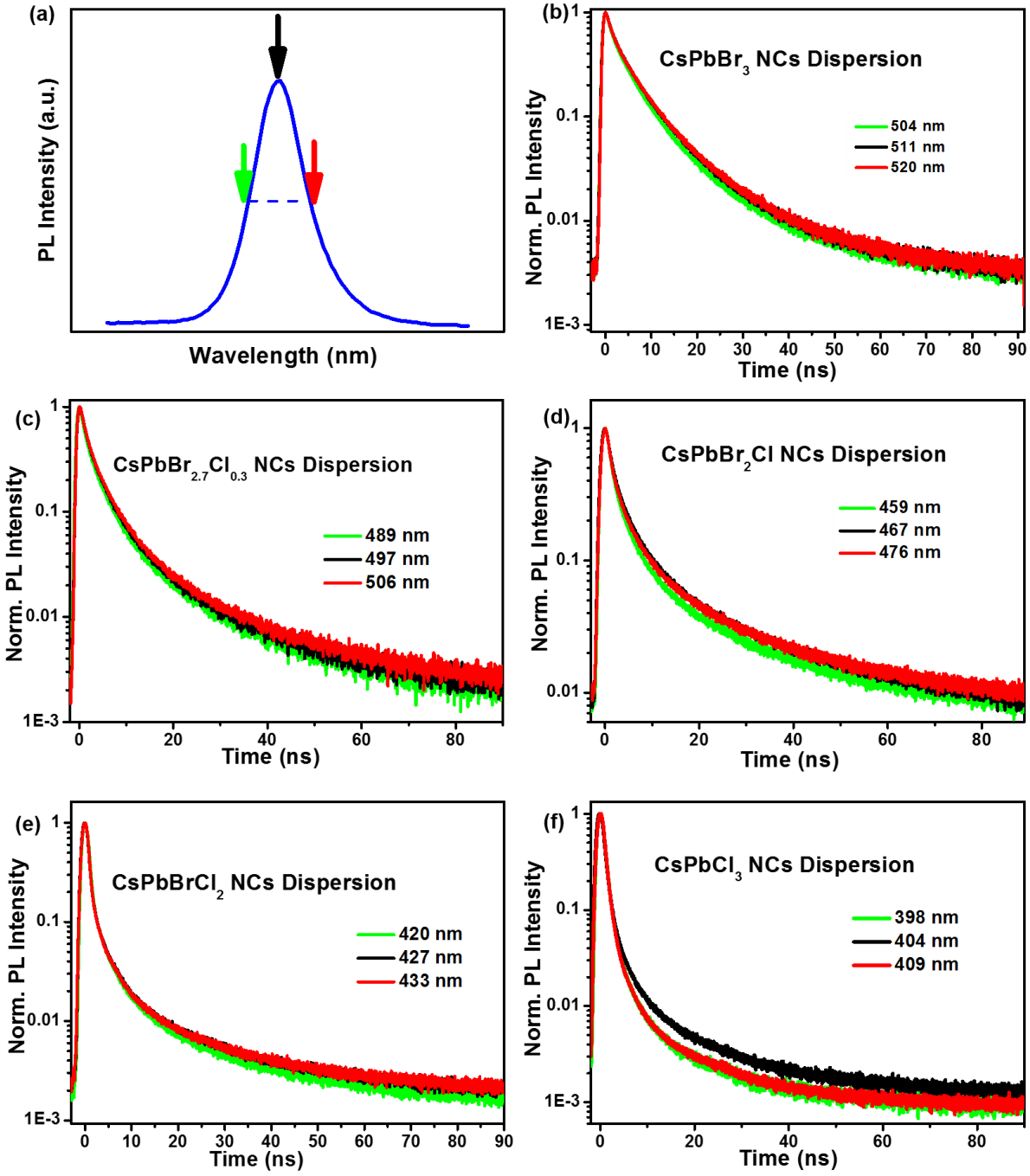

Figure 3.11: PL decay plots for various compositions of $CsPbX_3$ NC solutions. (a) A representative PL spectrum and the arrows represent the emission energies at which decay is monitored. (b)-(f) PL decay plots for solutions of (b) $CsPbBr_3$, (c) $CsPbBr_{2.7}Cl_{0.3}$, (d) $CsPbBr_2Cl$, (e) $CsPbBrCl_2$ and (f) $CsPbCl_3$ NCs respectively.

For all samples, similar decay pattern at various emission energies for both dispersion (solution) and film shows that the composition is homogeneous within the samples. The decay pattern shows that for all the compositions of $CsPbX_3$ (X = Br, Cl) NCs

there is less influence of FRET on governing the chromaticity of the NCs. Our claim here is that FRET and self-absorption remain in the same extent for both solution and films of $CsPbX_3$ NCs. If this is consistent over a long concentration range, then color of sample does not change with concentration and is an advantage in application point of view. For example, in the case of CdSe NCs, a film has a red-shifted PL with respect to its colloidal solution. Then, as the concentration increases (while preparing LEDs etc), the PL spectra gets hugely red-shifted and the chromaticity changes. Suppose, if there is contribution of FRET already in the solution due to some aggregate formation, then the extent of FRET the films will be having is similar to the extent in solution. Therefore, it does not largely affect the chromaticity of a material.

The PL decay profile is fitted for $CsPbX_3$ (X = Br, Cl, Br/Cl) NC films at the peak position using bi-exponential decay: $I(t) = a_1\exp(-t/\tau_1) + a_2\exp(-t/\tau_2)$ and the average lifetime is calculated as $\tau_{avg} = \sum a_i\tau_i^2/\sum a_i\tau_i$. The fit parameters are listed in Table 3.2.

Sample	a_1	τ_1 (ns)	a_2	τ_2 (ns)	τ_{avg} (ns)
$CsPbBr_3$	0.84	4.1	0.16	11.5	6.7
$CsPbBr_{2.7}Cl_{0.3}$	0.92	2.4	0.08	10.8	4.8
$CsPbBr_2Cl$	0.91	1.98	0.09	10.1	4.7
$CsPbBrCl_2$	0.95	1.03	0.05	10.5	4.3
$CsPbCl_3$	0.91	1	0.09	6.6	3.2

Table 3.2: PL decay fit data of all the compositions of $CsPbX_3$ (X = Br, Cl) NC films.

$CsPbBr_3$ NCs show radiative decay with an average lifetime of 6.7 ns. For Br-rich samples, only radiative pathways exists, but as the chloride composition increases, the average lifetime decreases as shown above in Table 3.2. As the lifetime decreases, the decay becomes faster and so, the decay profiles become steeper as the chloride composition increases. Also we can see that in Cl-rich samples, somehow non-radiative decay pathways come up. $CsPbBrCl_2$ and $CsPbCl_3$ NCs have non-radiative pathways present (decay pathways around 1 ns or lower is assigned as occurrence of non-radiative pathways). This also explains the QY data where Br-rich samples in $CsPbX_3$ NCs had high efficiency around 77% and with Cl-rich samples, there was a drastic decrease in efficiency to <10% due to the introduction of the non-radiative pathways. So, the decay fit data complements the trend in QY observed.

Electronic structure of $CsPbX_3$ NCs

In case of conventional p-s semiconductors, CBM is mostly comprised of *s*-states of cation and anion, and VBM mostly by *p*-states of the anion. This causes the CBM to be more dispersive than VBM as the s-orbitals are more delocalized than the p-orbitals here. So, the effective mass of the electron becomes smaller as compared to the effective mass of the hole, which leads to higher mobility of electrons than the holes[34].

But in the case of $CsPbX_3$ NCs, they have an "inverted" electronic structure as shown in the Figure 3.13. This unique electronic structure arises due to the presence of lone pair of electrons in the Pb *s*-orbital. So, due to presence of *s*- and *p*-states in the VBM, the coupling between s- and p- orbitals makes the VBM of perovskite NCs dispersive and the effective masses of electrons and holes get balanced. This leads to similar mobilities of electrons and holes and the probability of electrons to get trapped decreases[34]. Also, similar effective masses of electrons and holes mean more overlap probability of electrons and holes.

Also, most of the trap states due to dangling bonds or other defects, will be present in the gap between bonding and antibonding states (as per Figure. 3.13). But as the electron-hole recombination is happening between the empty state and antibonding state, defect-related non-radiative quenching of emission would be less and so, these NCs in general, exhibit high quantum efficiency.

Lambrescht et al. has reported a similar "inverted" electronic structure in the case of $CsSnI_3$ perovskite structure[33]. The explanation for $CsSnI_3$ can be extrapolated for $CsPbX_3$ also as both Pb and Sn lie in the same group and has a lone pair of electrons in the s-orbital, which is the basic reason for this unique band structure. It was indicated that the optical gap is mostly intra-atomic between Sn *s* and Sn *p* states. The unique nature of VBM and CBM could explain many of the intrinsic properties of these types of materials. They show strong optical transitions because the transitions between VBM and CBM has $\Delta l = 1$, which corresponds to an allowed transition. Also, the optical gap is actually determined by the antibonding covalent interaction of Sn *s* and I *p* orbitals. As the temperature increases, it is expected that this interaction gets weaker, thus the VB width gets decreased and hence, the optical gap increases[33].

Considering a similar example of $CH_3NH_3PbBr_3$, the Density of states (DOS) and Partial density of states (PDOS) plots are provided (Figure 3.12), just to have a look

at the contribution of each atomic orbitals in the VB and CB[35] that gives a better picture of the inverted band structure.

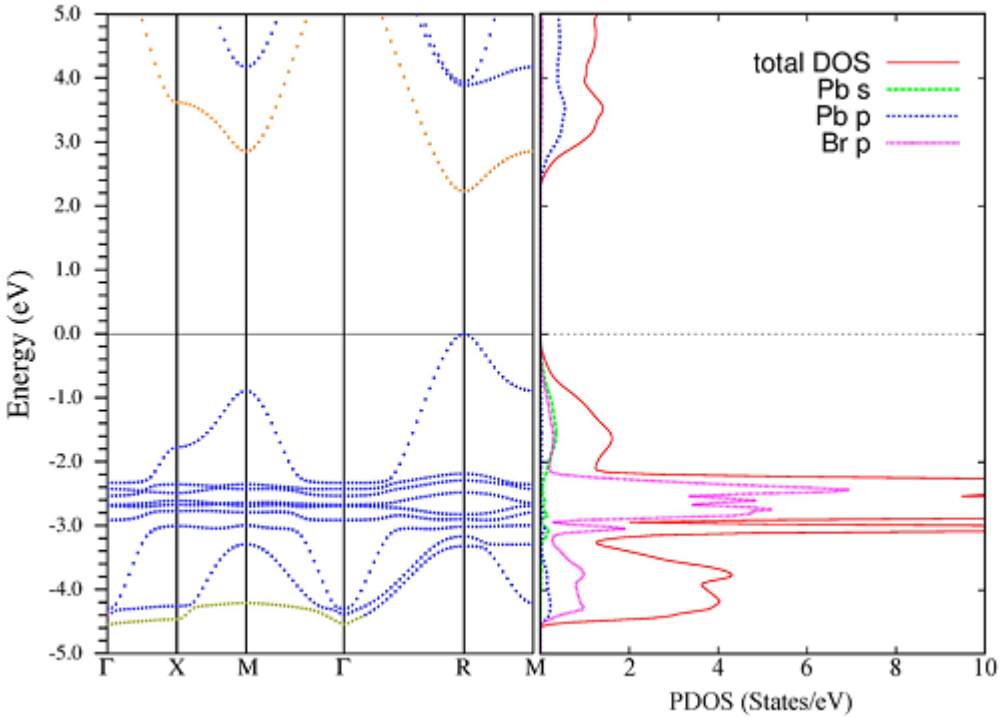

Figure 3.12: Band structure and partial densities of states of $CH_3NH_3PbBr_3$ (Adapted with permission from Jishi et al[35]. Copyright (2014) American Chemical Society)

A simplified schematic to show the unique "inverted" band structure of Pb-based metal halide perovskites (for example, $CsPbBr_3$ is being considered for the schematic) is provided below in Figure 3.13 for easy understanding.

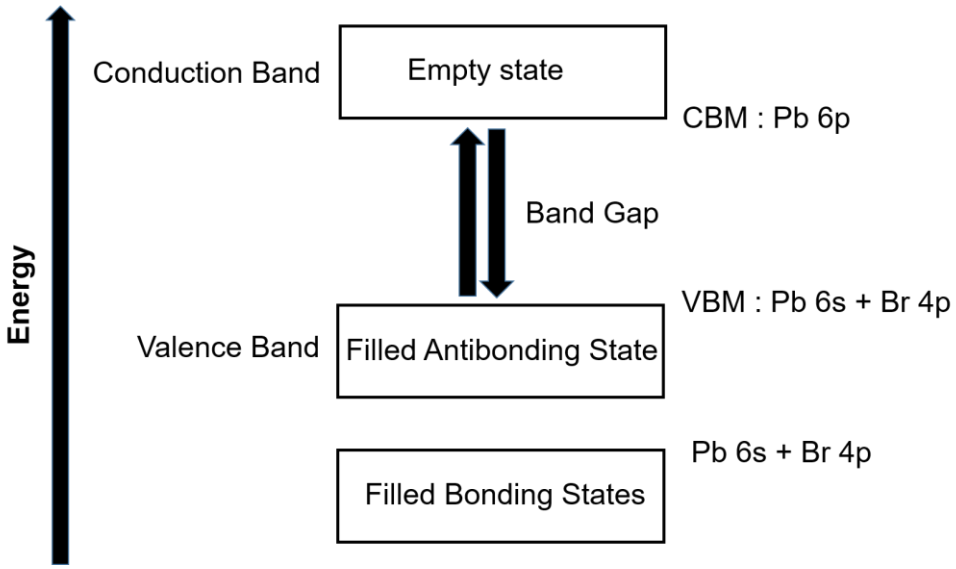

Figure 3.13: A simplified "inverted" band structure of $CsPbX_3$ NCs.

Conclusions

Various compositions of $CsPbX_3$ (X = Br, Cl) were synthesized. These compositions were characterized by XRD, EDAX Analysis and TEM. Tunability of absorption and emission spectra was achieved in the wavelength range of 400-515 nm. As chloride composition was increased in $CsPbX_3$ (X = Br, Cl, Br/Cl) NCs, a decrease in PL intensity and an increase in band gap were observed. It was also observed that a high QY (55-80%) was obtained when x in $CsPbBr_xCl_{3-x}$ was kept above 2. A narrow FWHM (75-95 meV) was also retained by all the experimental compositions of $CsPbX_3$ NCs that suggests purity of the emission color. The temperature dependent photoluminescence studies of colloidal $CsPbX_3$ NCs show an anomalous behaviour of either no change or a slight blue shift (upto 2-3 nm) in the PL peak position with an increase in temperature from 20 ^oC till 80 ^oC unlike traditional CdSe based cQDs, where it gets red-shifted with increase in temperature. PL spectra of close packed thin films and their solution dispersed samples were found to be similar in terms of the peak position and spectral width. Also, PL decay dynamics of close-packed thin films of $CsPbX_3$ NCs show similar PL decay at all emission energies, which suggest negligible influence of FRET on the chromaticity of the material. So, it is shown that both temperature and concentration of NCs does not affect chromaticity of the NCs to an extent (there is slight variation in both the cases, but very little as compared to the traditional QDs. These appealing PL properties along with the compositional tunability of $CsPbX_3$ NCs substantiate their efficiency over traditional CdSe based CQDs, and therefore, are better potential candidates for ultra-high definition displays. The advantageous PL properties of $CsPbX_3$ NCs can be attributed to the proposed “inverted” band structure of metal halide perovskites. Now, further studies have to be done to extend the emission properties to lower energies using X = Br/I, I in $CsPbX_3$ NCs.

References

[1] Kojima, A.; Teshima, K.; Shirai, Y.; Miyasaka, T. Oraganometal halide perovskites as visible-light sensitizers for photovoltaic cells. *J. Am. Chem. Soc.* **2009**, *131*, 6050– 6051.

[2] Lee, M. M.; Teuscher, J.; Miyasaka, T.; Murakami, T. N.; Snaith, H. J. Efficient Hybrid Solar Cells Based on Meso-Superstructured Organometal Halide Perovskites. *Science* **2012,** *338*, 643-647.

[3] Stranks, S. D.; Snaith, H. J. Metal-halide perovskites for photovoltaic and light-emitting devices. *Nat Nanotechnol.* **2015**, *10*, 391-402.

[4] Tan, Z. K.; Moghaddam, R. S.; Lai, M. L.; Docampo, P.; Higler, R.; Deschler, F.; Price, M.; Sadhanala, A.; Pazos, L. M.; Credgington, D.; Hanusch, F.; Bein, T.; Snaith, H. J.; Friend, R. H. Bright light emitting diodes based on organometal halide perovskite. *Nat Nanotechnol.* **2014,** *9*, 687-692.

[5] Kagan, C. R.; Mitzi, D. B.; Dimitrakopoulos, C. D. Organic-inorganic hybrid materials as semiconducting channels in thin-film field-effect transistors. *Science* **1999**, *286*, 945-947.

[6] Guo, Y. L.; Liu, C.; Tanaka, H.; Nakamura, E. Air-Stable and Solution-Processable Perovskite Photodetectors for Solar-Blind UV and Visible Light. *J. Phys. Chem. Lett.* **2015,** *6*, 535-539

[7] Schmidt, L. C.; Pertegas, A.; Gonzalez-Carrero, S.; Malinkiewicz, O.; Agouram, S.; Espallargas, G. M.; Bolink, H. J.; Galian, R. E.; Perez-Prieto, J. Nontemplate Synthesis of $CH_3NH_3PbBr_3$ Perovskite Nanoparticles. *J. Am. Chem. Soc*. **2014**, *136*, 850-853.

[8] Zhang, F.; Zhong, H.; Chen, C.; Wu, X. G.; Hu, X.; Huang, H.; Han, J.; Zou, B.; Dong, Y. Brightly luminescent and color tunable colloidal $CH_3NH_3PbX_3$ (X = Br, I, Cl) quantum dots: potential alternatives for display technology. *ACS Nano*, **2015**, *9*, 4533–4542

[9] Møller, C. K. Crystal structure and photoconductivity of caesium plumbohalides. *Nature* **1958**, *182*, 1436 – 1436.

[10] Nitsch, K.; Hamplovfi, V.; Nikl, M.; Polgk, K.; Rodovfi, M. Lead bromide and ternary alkali lead bromide single crystals - growth and emission properties. *Chem. Phys. Lett.* **1996,** *258,* 518-522.

[11] Heidrich, K.; Kunzel, H.; Treusch, J. Optical properties and electronic structure of $CsPbCl_3$ and $CsPbBr_3$. *Solid State commun*. **1978,** *25,* 887-889.

[12] Somma, F.; Nikl, M.; Nitsch, K.; Fabeni, P.; Pazzi, G. P. Excitons in $CsPbX_3$ (X = Cl, Br, I) ternary nanocrystallites in thin films matrices. *J. Lumin.* **2001,** *94–95,*169–172.

[13] Protesescu, L.; Yakunin, S.; Bodnarchuk, M.I.; Krieg, F.; Caputo, R.; Hendon, C.H.; Yang, R.X; Walsh, A., Kovalenko, M. V. Nanocrystals of cesium lead halide perovskites ($CsPbX_3$, X = Cl, Br, and I): novel optoelectronic materials showing bright emission with wide color gamut. *Nano Lett.* **2015**, *15*, 3692–3696.

[14] Swarnkar, A.; Chulliyil, R.; Ravi, V. K.; Irfanullah, M.; Chowdhury, A.; Nag, A. Colloidal $CsPbBr_3$ Perovskite Nanocrystals: Luminescence beyond traditional quantum dots. *Angew. Chem. Int. Ed.* **2015**, *54*, 15424–15428.

[15] Glazer, A. M. The classification of tilted octahedra in perovskites*. Acta Cryst* **1972**, *B28*, 3384-3392.

[16] Roth, R.S; Classification of perovskite and other ABO_3–type compounds. *J Res Natl Bur Stand* **1957**, *58,* 75-88.

[17] Kay, H. F.; Bailey, P.C. Structure and Properties of $CaTiO_3$. *Acta. Cryst.* **1957**, *10*, 219-226.

[18] Navrotsky, A. Energetics and Crystal Chemical Systematics among Ilmenite, Lithium Niobate, and Perovskite Structures. *Chem. Mater.* **1998**, *10,* 2787-2793.

[19] Mitzi, D. B. Templating and structural engineering in organic–inorganic perovskites. *J. Chem. Soc. Dalt. Trans.* **2001**, 1–12 (2001)

[20] Shi, J. W.; Guo L. J. ABO_3-based photocatalysts for water splitting. *Prog. Nat. Sci. Mater. Int.* **2012**, *22*, 592–615

[21] https://crystallography365.wordpress.com/2014/01/22/the-first-perovskite-calcium-titanate/

[22] Ekimov, A. I.; Hache, F.; Schanne-Klein, M.C.; Ricard, D.; Flytzanis, C.; Kudryavtsev, I. A.; Yazeva, T. V.; Rodina, A.V.; Efros, Al. L. Absorption and intensity-dependent photoluminescence measurements on CdSe quantum dots: assignment of the first electronic transitions. *J. Opt. Soc. Am. B.* **1993**, *10*, 100-107.

[23] Murray, C. B.; Kagan, C. R.; Bawendi, M.G. Synthesis and characterization of monodisperse nanocrystals and close-packed nanocrystal assemblies. *Annu. Rev. Mater. Sci.* **2000,** *30*, 545–610.

[24] Wahl, M. PicoQuant GmbH, Rudower Chaussee 29, 12489 Berlin, Germany, Time-Correlated Single Photon Counting.

[25] Lakowicz, J. R. Principles of fluorescence spectroscopy. *Springer*, **2006**.

[26] https://www.edinst.com/techniques/time-resolved-fluorescence/

[27] Rodová, M.; Brožek, J.; Knížek, K.; Nitsch, K. Phase transitions in ternary caesium lead bromide. *J. Therm. Anal. Calorim.* **2003**, *71*, 667-673

[28] Møller, C.K. A phase transition in caesium plumbochloride. *Nature* **1957**, *180,* 981-982.

[29] Goldstein, J. Scanning Electron Microscopy and X-Ray Microanalysis. *Springer,* **2003.**

[30] White, A. M.; Williams, E. W.; Porteous, P.; Hilsum, C. Applications of photoluminescence excitation spectroscopy to the study of indium gallium phosphide alloys *J. Phys. D: Appl. Phys.* **1970**, 3, 1322-1328.

[31] Instruction manual, TLC 50, Temperature-Controlled Cuvette Holder for fluorescence; Quantum North West.

[32] Yu, C.; Chen, Z.; Wang, J. J.; Pfenninger, W.; Vockic, N.; Kenney, J. T.; Shum, K. *J.* Temperature dependence of the band gap of perovskite semiconductor compound $CsSnI_3$ *Appl. Phys.* **2011**, *110*, 063526.

[33] Huang, L. Y.; Lambrecht, W. R. L. Electronic band structure, phonons, and exciton binding energies of halide perovskites $CsSnCl_3$, $CsSnBr_3$, and $CsSnI_3$ *Phys. Rev. B* **2013**, *88*, 165203.

[34] Wen, X.; Baillie, A. H.; Huang, S,; Sheng, R.; Chen, S.; Ko, H.; Green, M. A. Mobile Charge-Induced Fluorescence Intermittency in Methylammonium Lead Bromide Perovskite. *Nano Lett.* **2015**, *15*, 4644–4649.

[35] Jishi, R. A.; Ta, O. B.; Sharif, A. A. Modeling of lead halide perovskites for photovoltaic applications. *J. Phys. Chem. C* **2014**, *118*, 28344-28349.
